Analysis and Design of Dielectric Resonator Rod Antenna at Terahertz Frequency for Next-Generation Communication System

Dissertation submitted in partial fulfillment of the

requirements for the Degree of

MASTERS OF TECHNOLOGY

By

KANISHKA KATOCH
Enrollment No: 152003

UNDER THE GUIDANCE OF

Prof. Ghanshyam Singh

DEPARTMENT OF ELECTRONICS AND COMMUNICATION ENGINEERING

JAYPEE UNIVERSITY OF INFORMATION TECHNOLOGY

WAKNAGHAT, SOLAN, H.P.

MAY-2017

TABLE OF CONTENTS

DECLARATION

I hereby declare that the work reported in the M-Tech dissertation entitled **"Analysis and Design of Dielectric Resonator Rod Antenna at Terahertz Frequency for Next-Generation Communication System"** submitted at **Jaypee University of Information Technology, Waknaghat, India,** is an authentic record of my work carried out under the supervision of **Prof. Ghanshyam Singh**. I have not submitted this work elsewhere for any other degree or diploma.

Kanishka Katoch
Department of Electronics and Communication Engineering
Jaypee University of Information Technology, Waknaghat, India
Date:

JAYPEE UNIVERSITY OF INFORMATION TECHNOLOGY
(Established by H.P. State Legislative vide Act No. 14 of 2002)
P.O. Waknaghat, Teh. Kandaghat, Distt. Solan - 173234 (H.P.) INDIA
Website: www.juit.ac.in
Phone No. (91) 01792-257999 (30 Lines)
Fax: +91-01792-245362

CERTIFICATE

This is to certify that the work reported in the M-Tech. dissertation entitled "**Analysis and Design of Dielectric Resonator Rod Antenna at Terahertz Frequency for Next-Generation Communication System**", submitted by **Kanishka Katoch** at **Jaypee University of Information Technology, Waknaghat**, **India,** is a bonafide record of her original work carried out under my supervision. This work has not been submitted elsewhere for any other degree or diploma.

Prof. Ghanshyam Singh

Department of Electronics and Communication Engineering

Jaypee University of Information Technology, Waknaghat, India

Date:

ACKNOWLEDGEMENT

I earnestly wish to express my heartfelt thanks and a sense of gratitude to my guide **'Dr. Ghanshyam Singh'**, Electronics and Communication Engineering Department, for his valuable guidance and constant inspiration in preparing this report. My frequent interactions with him in all aspects of the report writing have been a great learning experience for me. I shall always cherish his support and encouragement.

I heartily appreciate Mr. Ashutosh Sharma, Mrs. Isha Malhotra, Mr. Prabhat Thakur and Ms. Jyotsna Dogra for helping me directly or indirectly in making these task a success. In this context, I would like to thank all the other staff members, both teaching and non-teaching.

Last but not the least, I would like to thank my parents (Pradeep Katoch and Asha) and my sister (Shreya Katoch) for their valuable support.

Kanishka Katoch

Date:

LIST OF PUBLICATIONS

[1] Kanishka Katoch and G. Singh, "Dielectric resonator antenna for next-generation communication — A holistic overview and future perspective", *Infrared Physics and Technology*, (Submitted), April 2017.

[2] Kanishka Katoch and G. Singh, "Analysis and design of dielectric resonator rod antenna at terahertz frequency for next- generation communication system", *Optics Communication*, (Submitted), April 2017.

[3] Kanishka Katoch and G. Singh, "Highly Directive dielectric resonator rod array antenna at terahertz frequency wireless communication", *IEEE Radio and Antenna Days of the Indian Ocean, Cape Town, S Africa, Sept. 25-28, 2017*, (Submitted).

ABSTRACT

The end users of next generation (5G) mobile communication networks requires a major paradigm shift to fulfill the increasing demand for higher data rates, low latencies, better spectral efficiency, high security, reliable connectivity and high scalability. The global bandwidth scarcity facing wireless carriers has motivated the exploration of the underutilized millimeter/terahertz wave frequency regime of the spectrum for future broadband cellular communication networks. The terahertz communication link is advantageous over microwave link and infrared link due to its wide bandwidth and less atmospheric losses, respectively. Therefore, using THz technology for next generation mobile communication networks can satisfy the desired needs. However, the high power sources are required to be developed within the atmospheric attenuation window as the power radiated by the THz source is very less.

In the field of wireless communication system, the dielectric resonator antennas (DRAs) are more promising for use in THz technology over microstrip antennas because of its features such as, low loss, low cost, small size, design flexibility, ease of excitation, and simple feeding techniques. Moreover, the DRA show high radiation efficiency and different radiation pattern at different mode with temperature stability and wide range bandwidth. The major limitation of the DRA is the low gain and directivity values which poses an operational constraint on its use in next generation mobile communication networks. Therefore, there is a necessity of designing a DRA using gain/directivity enhancement techniques.

To enhance the gain of the DRRA, the implementation of its array is beneficial for communication. At terahertz frequency, the dimension of the antenna becomes smaller therefore a number of single element DRAs are designed to form an array. For the validation of the designed DRRA array configuration, the frequency downscaling technique is purposed. Moreover, to increase the impedance bandwidth of the DRRA, tapering of the radiating source is implemented which also helps to shift the operating frequency of antenna to higher values. This is advantageous in applications wherein shift in the transmission band for communication is needed. Further, in the communication application, the scanning of beam over a large coverage area with optimum gain is required. The switching of beam is achieved by using the concept of beam-steering in the proposed DRRA array.

LIST OF ABBREVIATIONS

THz	Terahertz
DR	Dielectric resonator
LTE	Long term evolution
DRA	Dielectric resonator antenna
MSA	Microstrip antenna
RDRA	Rectangular dielectric resonator antenna
CDRA	Cylindrical dielectric resonator antenna
HDRA	Hemispherical dielectric resonator antenna
DRRA	Dielectric resonator rod antenna
UWB	Ultra-wide band
NB	Narrow band
CP	circular polarization
LP	Linear polarization
DDPA	Dense dielectric patch antenna
WPD	Wilkinson power divider

LIST OF FIGURES

LIST OF TABLES

CHAPTER-1

INTRODUCTION

Over the past few decades, the demand for high data rate in continuously increasing for faster, smarter and safer wireless communication system. The present communication system provides 100 Mbps data rate with 15 ms roundtrip latency of the data plan in the LTE network. However with the exponential increase in the demand of the end users, a significant shift is required to further strengthen the present communication system, since there is a bottleneck faced in the spectrum resources, making it difficult to achieve better performance in scarce bandwidth. The idea is to increase the data rate by increasing the bandwidth. There are possibly two ways to do so such as 1) by increasing the bandwidth, however the system itself is inherited with narrow bandwidth and the maximum usable bandwidth of the device is approximately 10% of its operating frequency and 2) by switching to higher operating frequency such that even the narrow band can get a wider bandwidth that is the best solution for the next generation communication. Therefore, in order to achieve higher data rate, there is a demand of high frequency spectrum with its efficient utilization. Moreover, for more flexibility small-cells with ultra-dense network will be deployed which ultimately leads for the 5G wireless communication system [3]-[6].

The 5^{th} generation communication system will support 10 Gbps peak data rate with 100 Mbps cell edge data rate, 1ms end-to-end latency, 1000 times decrease in energy consumption per bit, high scalability by accommodating 50 billion devices, improving cell edge users connectivity and high security [3]. These resources can only come from additional spectrum. The use of higher frequency, i.e., millimeter wave (30 GHz to 300 GHz) is therefore gaining momentum [6]-[8]. However, the limited available bandwidth (7 GHz) poses a constraint on the maximum available data rate. According to the Edholm's law of bandwidth, by 2020 the terabit-per-second link will become reality. With 7GHz of bandwidth the spectral efficiency of 100 bits/s/Hz becomes unrealistic to be achieved. Therefore, there is need to shift the focus on "beyond 5G" (5G+) networks where the terahertz frequency band is the key technology, which is envisioned to alleviate the spectrum scarcity and capacity limitation of the current wireless communication system [2].

The terahertz frequency extends from 0.1 THz to 10 THz, sandwiched between well explored microwave and far infrared regime of the spectrum. The unavailability of the detectors, power sources and other hardware led this band rather untouched by the researchers and named as terahertz band gap. However, from last few decades, due to scarcity of resources and exponential growth of semi-conductor technology the band got noticed.

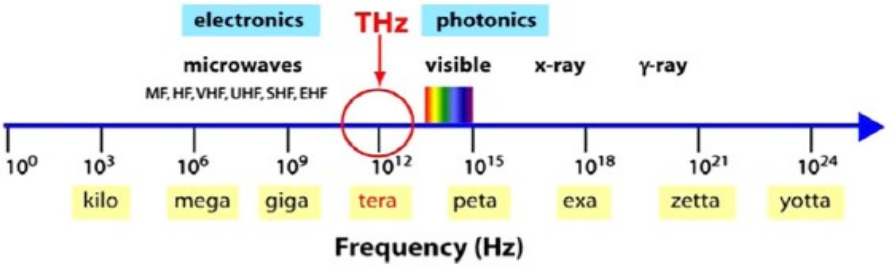

Figure 1.1: The position of terahertz band in the between microwave and infrared spectrum [5]

Since this band lies uniquely in between the microwave and far-infrared regime of the spectrum and it inherits the electronic as well as photonic properties. There are various advantages related to the terahertz region with respect to microwave and infrared region [1]-[4].

- Terahertz range comprises of wider bandwidth than that of the microwave range which has a limited bandwidth and almost pre-occupied for different services.
- The diffraction in terahertz band of the spectrum is less than that of the microwave band, therefore the beam is highly directional and has an advantage in line-of-sight communication.
- It upholds large channel bandwidth for spread spectrum communication and provides a secure communication.
- The THz wave attenuation in certain atmospheric conditions, such as fog, is less in comparison to that of the infrared wave, therefore the THz band provides a reliable communication.
- In the infrared communication system, the scintillation effect increases. Hence THz communication system can be used to reduce it.
- The terahertz frequency range is unregulated by regulatory authorities. 250 GHz is the maximum allocated frequency and above it the band is license free.

- The scattering of the wave depends on the wavelength, therefore the THz wave scatters less than that of the light wave.
- THz band provides better resolution as the frequency increases.
- It exhibits low ionization effect on the human tissues due to its low power level, therefore the terahertz can be used for imaging than the X-rays.

However, there are various constraints associated with the terahertz frequency band, which are listed as follows [1]-[4]:

- According to the Friis transmission equation, the received power depends upon the frequency and the transmission path. As the frequency increases the received power decreases and to compensate it the transmission path is required to be kept small which posses a constraint for long haul communication.
- The THz frequency attenuates more often even by human body and material such as brick, furniture. Therefore, THz wave is more vulnerable to shadowing than microwaves.
- The atmospheric attenuation of THz wave occurs due to its absorption by water molecules present in the environment.
- The scarcity of highly developed infrastructure such as transceivers, detectors, sensors, sources, etc is the major huddle for THz communication.

While focusing on the high data rate, with high bandwidth, the characteristics of the device changes. The conventional microstrip antenna (MSA) system becomes more susceptible to the conductor losses at higher frequencies due to the skin depth effect and provides narrow impedance bandwidth and low efficiency for the communication making it least usable at higher microwave frequencies or above. A radiator with least losses is required with wider impedance bandwidth, high efficiency and high gain, so that a good communication network can be established. Therefore, the dielectric resonator antenna (DRA) emerged as a better choice than that of the MSA.

Lai et. al. [9] have compared the radiation efficiency of dielectric resonator antenna and microstrip antenna at 35 GHz. The effect of both sampling interval and cross-polarization is taken into account and it is observed that both the proposed antennas resonate at 35.2 GHz (MSA) and

35.5GHz (DRA), respectively. The bandwidth of DRA is significantly more than MSA, while the radiation pattern is slightly broader. The DRA can radiate more efficiently but if the directivity is considered then MSA is more useful as shown in Table 1.1.

Table 1.1: The performance comparison [9].

Radiation parameters	CDMA		CDRA	
	Simulated value	Measured value	Simulated value	Measured value
Bandwidth (S_{11}<-10dB)	3.7%	2.6%	18.6%	15.6%
Efficiency	81.8%	78.2%	95.2%	94.9%
Peak Directivity (dBi)	7.6	8.6	6.1	7.6
Peak Gain (dB)	6.7	7.1	6.0	6.9

1.1 Basics of Dielectric Resonator Antenna

Before 1983, the dielectric resonators [10] were predominantly used in microwave circuit as filters and oscillators. The low-loss high permittivity materials, with dielectric constant $\epsilon_r > 20$ and unloaded Q-factor in between 50 and 500, which increases as high as 10,000, were cut out for the operations for working at the higher order modes. The lower modes were not preferred due to the radiation losses which led to the design of first DRA, introduced by Long et. al. in 1983 [11] in that a cylindrical DR was mounted over the metallic ground plane and excited at its fundamental mode. The idea was to design an antenna which could work at millimeter wave frequency as for many devices the frequency of interest was shifting upwards.

Subsequently, the rectangular DRA [12] and hemispherical DRA [13] were studied, which serves as the basic structures. The DRA is best suited for millimeter and sub-millimeter frequency range than that of the conventional microstrip patch antenna due to its compact size, low dielectric losses, low profile, high temperature tolerance, high versatility in its shape, high efficiency, wide impedance bandwidth and high flexibility in excitation techniques [14]-[16]. The losses associated with DRA are mainly due to the imperfect dielectric material, which is very small in

practice. Further, the other shapes such as triangular [17], cylindrical-ring [18-19] and spherical-cap [20] were also studied, as shown in Figure 1.2.

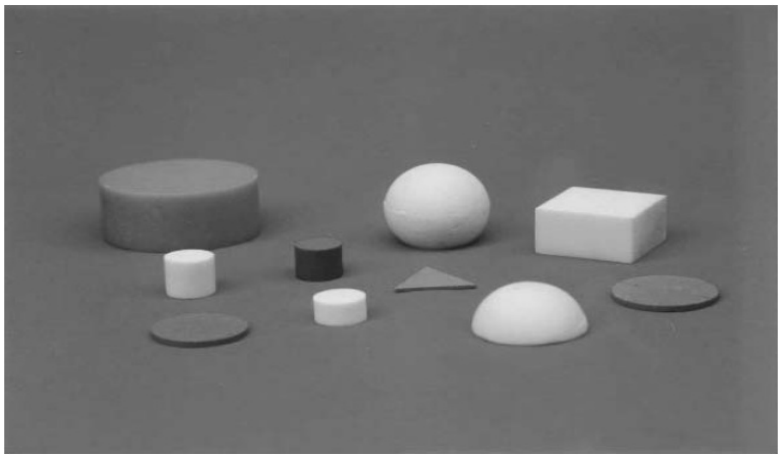

Figure 1.2: Different shapes of DRA [18].

1.2 Canonical DRAs

The canonical DRAs are mainly classified as hemispherical DRA, rectangular DRA and cylindrical DRA.

1.2.1 Hemispherical DRA

Due to the simple structure, the hemispherical DRA (HDRA) is particularly popular for theoretical analysis, as shown in Figure 1.3(a). The HDRA supports transverse electric TE_{nmr} modes and transverse magnetic TM_{nmr} modes, where *n* denotes the order of variation of elevation field, *m* denotes the order of variation of azimuth field and *r* is the radial direction field. For the values $m \leq n$, both the transverse modes have the same resonant frequency [16]. Therefore, it poses a limit for various practical applications due to the degeneracy of the modes and is least commonly used in comparison to other basic DRA structures. The most commonly excited lower order HDRA modes are the TE_{111}, TE_{101} and TM_{101}. These three modes radiates like horizontal magnetic dipole, axial magnetic dipole and axial electric dipole, respectively.

1.2.2 Rectangular DRA

The rectangular DRA (RDRA) is more advantageous than that of HDRA and CDRA due to **1)** two independent shape parameters, therefore more degree of freedom, **2)** the degeneracy of the modes can be avoided by controlling the dimensions and **3)** it provides design flexibility for optimum bandwidth [12]. The structure is shown in Figure 1.3(b) which has two independent aspect ratios (width/length or height/length) for design to be more flexible for a given dielectric permittivity of the material and resonance frequency in terms of bandwidth [16]. The TE_{111} is the fundamental mode of the RDRA and resonates like a short dipole.

1.2.3 Cylindrical DRA

The cylindrical DRA (CDRA) is the extensively used DRA in the practical scenario due to its cheaper and easier fabrication in comparison to that of the RDRA and HDRA, as shown in Figure 1.3(c). It has more degree of freedom than that of HDRA and supports three type of modes, i.e., the transverse electric TE_{npm}, the transverse magnetic TM_{npm} and the hybrid modes HEM_{npm}, where n, p and m denotes the number of field variations in azimuth plane, radial direction and z-direction. The most commonly excited modes are the $HEM_{11\delta}$, the $TE_{01\delta}$ and the$TM_{01\delta}$. These modes radiates as horizontal magnetic dipole, vertical magnetic monopole and vertical electric monopole, respectively. Here δ indicates that the DR is shorter than the one-half of the wavelength.

For a cylinder of height 'h', radius 'a', the field distribution can be described in terms of Bessel function and given as:

$$TE \text{ mode: } H_z^{npm} = J_n\left\langle\left(X_{np}^{TE} r\right)| a\right\rangle\begin{Bmatrix}\sin(n\phi)\\ \cos(n\phi)\end{Bmatrix}\sin[(2m+1)\pi z/2h] \tag{1.1}$$

$$\text{TM mode: } E_z^{npm} = J_n\left\langle\left(X_{np}^{TM} r\right)| a\right\rangle\begin{Bmatrix}\sin(n\phi)\\ \cos(n\phi)\end{Bmatrix}\sin[(2m+1)\pi z/2h] \tag{1.2}$$

where n = 1, 2…. p = 1, 2…. m = 0, 1,…. J_n is the n^{th} order ordinary Bessel function of first kind whereas $\left(X_{np}^{TE}\right)$and $\left(X_{np}^{TM}\right)$are the roots such that following corresponding characteristic Equations satisfy:

$J_n\left(X_{np}^{TE}\right)=0$ and $J_n\left(X_{np}^{TM}\right)=0$

The simplified Equation is given by:

$$f_{npm}=\frac{C}{2\pi a\sqrt{\varepsilon_r}}\sqrt{\left\{\begin{matrix}X_{np}^{TE^2}\\X_{np}^{TM^2}\end{matrix}\right\}+\left[\frac{\pi a}{2d}(2m+1)\right]^2} \tag{1.3}$$

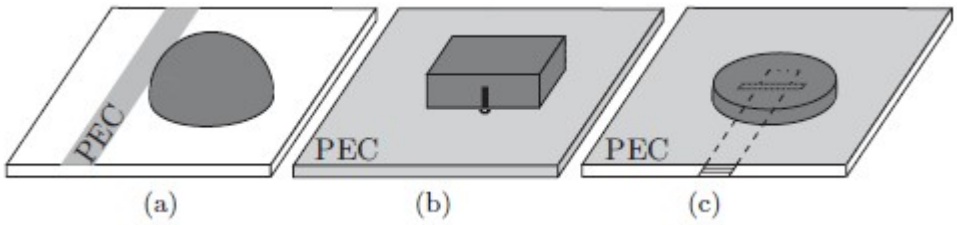

Figure 1.3: The canonical structures of the DRA (a) hemispherical DRA fed through a microstrip-line (b) rectangular DRA fed by coaxial probe and (c) cylindrical DRA fed by aperture slot.

1.3 Coupling of DRA.

The energy coupling scheme plays an important role in the design of the practical DRA. The location and type of coupling affects the performance of antenna in terms of mode excitation, radiation pattern, polarization and impedance bandwidth. The amount of coupling is determined Lorentz reciprocity theorem and is given by:

$$k \propto \int (\vec{E}.\vec{J}_E)dV \tag{1.4}$$

$$k \propto \int (\vec{H}.\vec{J}_M)dV \tag{1.5}$$

where k is the coupling constant, E and H are the electric and magnetic field intensity, respectively. J_E and J_M are the electric and magnetic currents, respectively. By equation 1.4 and 1.5, it is pointed that for achieving strong coupling in between the DRA and electric or magnetic current source, the source should be positioned in the strongest premise of the electric or magnetic field of the DRA mode. The basic feeding techniques are listed as follows.

1.3.1 Coaxial probe

A metallic probe is positioned vertically to achieve a strong coupling to the DRA. By adjusting the height and diameter of the probe the level of coupling is optimized. Various modes get excited according to the probe location and different shapes of the DRA, for example, when it fed axially, the TM modes only get excited. If the probe is located at the centre of the DRA, the TM_{01} mode gets excited whereas if the probe is positioned at the peripheral of the DRA, HEM_{11} (TEM_{110}) mode gets excited as shown in Figure 1.4. This is simplest mechanism which direct 50Ω impedance matches without using matching networks [21-23].

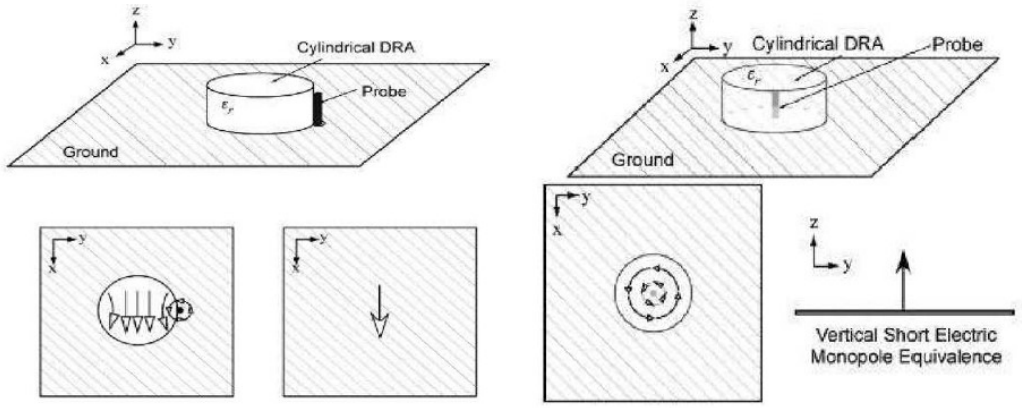

Figure 1.4: The excitation of magnetic and electric current in DRA [16].

1.3.2 Microstrip line

This is the simplest feeding method. The antenna behaves as a short horizontal magnetic dipole, as shown in Figure 1.5. By varying the parameter '*s*' or changing the dielectric constant of DRA, the level of coupling can be enhanced [16]. However, at low dielectric constant, minimum energy is coupled [24]. Further, the major limitation is at higher frequencies where the spurious radiation occurs due to skin depth effect and results reduction of impedance bandwidth and cross-polarization [25].

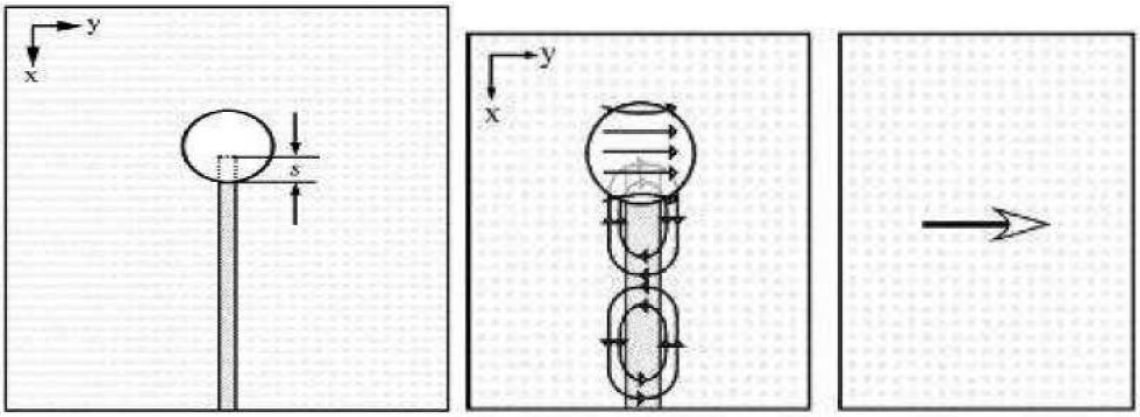

Figure 1.5: Field distribution in DRA using microstrip line [16].

1.3.3 Aperture slot

To avoid the unwanted radiation, the aperture slot feed network is located below the ground plane. The aperture when located at the centre of the DRA, the antenna behaves like a magnetic dipole and excites the fundamental HEM_{11} (TM_{110}) mode. The slot is fed by a microstrip line to seek good impedance matching. The slot dimensions kept small to reduce the backward radiation and to couple the energy efficiently [26-28].

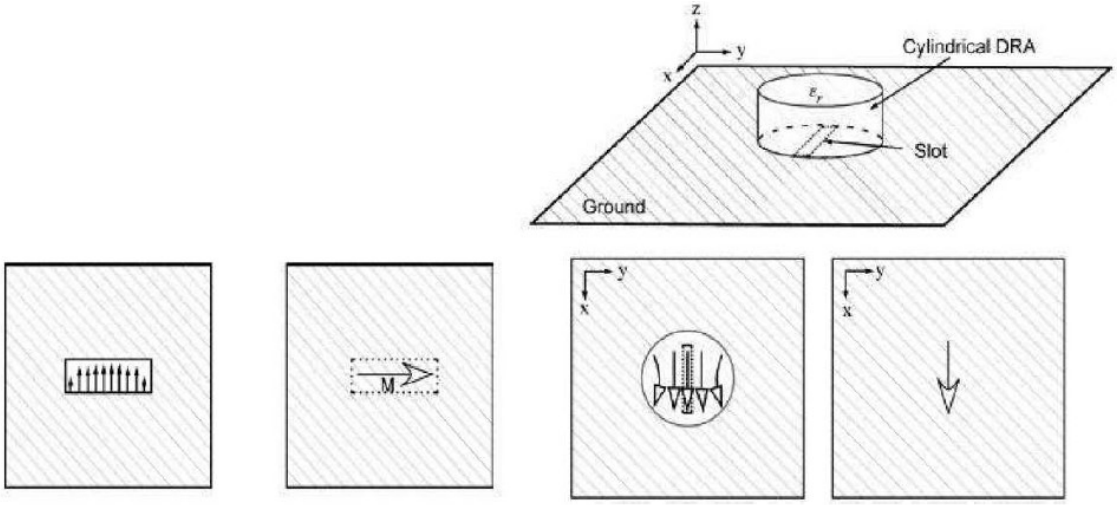

Figure 1.6: Field distribution using aperture feeding [16].

1.3.4 Coplanar waveguide

The energy is coupled to DRA by using coplanar loops. The desired coupling level is achieved by sliding the DR over the loop. By sliding the loop from the edges to the centre of the DRA either $HE_{11\delta}$ mode or TE011 mode gets excited of the cylindrical DRA [29-32], as shown in Figure 1.7.

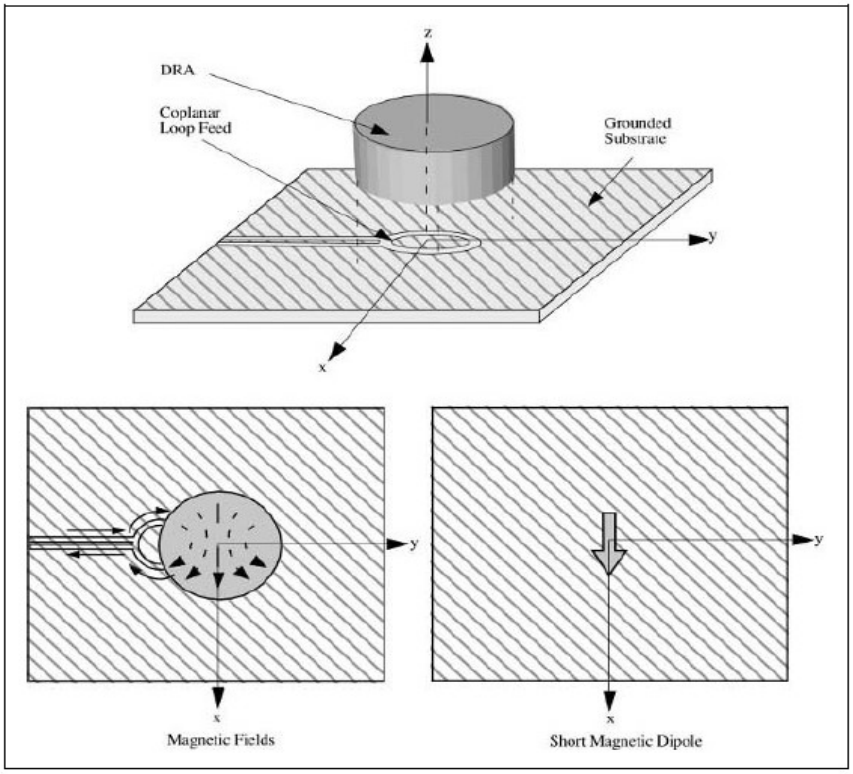

Figure 1.7: Field distribution using coplanar waveguide [16].

1.3.5 Dielectric imaging waveguide

At higher microwave/millimeter wave frequencies, the dielectric image guide is the best solution due to minimum dielectric losses. To enhance the coupling, a higher permittivity material is chosen, as shown in Figure 1.8. It is best suited because it can be utilized for series as well as linear array antenna design [33].

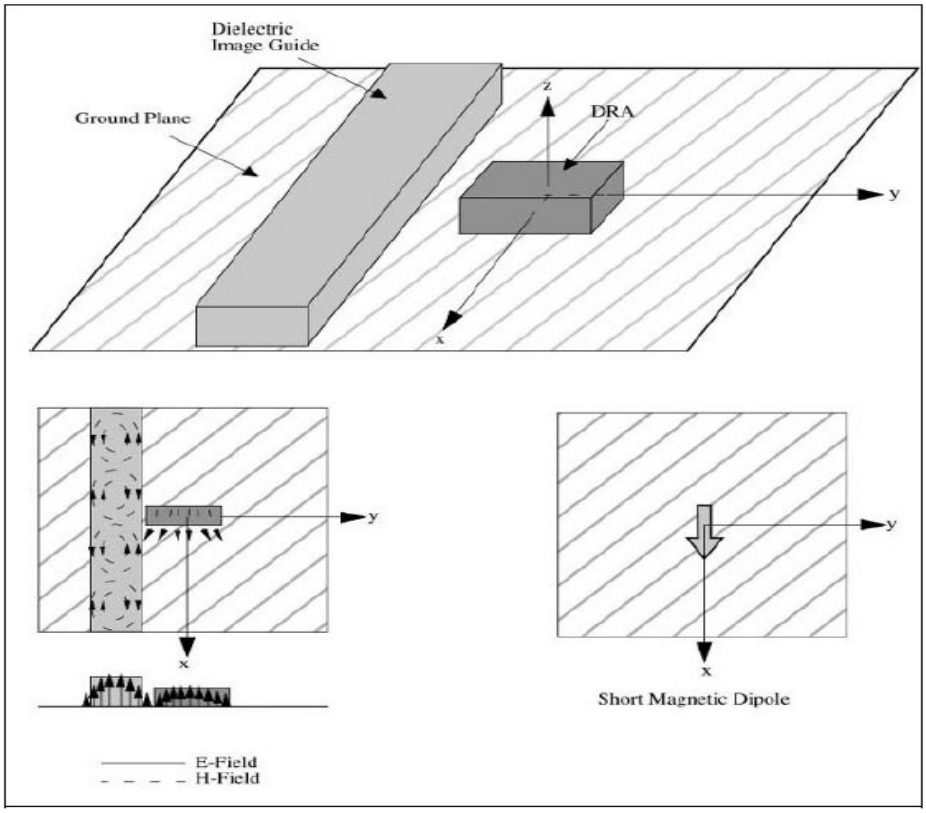

Figure 1.8: Field distribution using dielectric imaging waveguide [16].

Kumar and Gupta [25] have compared microstrip line, coaxial probe, aperture slot and coplanar waveguide feedings and concluded that the coaxial probe feeding provides better impedance bandwidth of 53.9% for S_{11}<-10 dB and provides the resonance dip of -36dB at 3.15GHz which is way better than any other feeding. On the other hand, Guha and Kumar [34] have compared MSA and DRA at 4 GHz and studied different feeding techniques for both the antennas operating near the same frequency such as coaxial probe, microstrip-line and rectangular aperture feeding, and demonstrated that the DRA is having wider bandwidth and higher efficiency than MSA however the gain of MSA is higher. However, with context to the cross polarization and radiation efficiency the aperture/microstrip-line feeding and coaxial probe is better, respectively.

1.4 DRA Array

The next generation communication system demands more data-rate as compared to the 4th generation and with single element antenna this cannot be obtained. By Shannon's capacity

formula, the enhanced data-rate can be achieved by either increasing the bandwidth of the system or by increasing the signal to noise ratio. At a particular bandwidth the data rate can be increased by increasing the signal's power and that can be achieved by increasing the gain of the system. As reported a single DRA is not capable of yielding more gain. Therefore, multiple antenna system is necessary for enhancing the antenna performance.

Various individual antennas are arranged with different configurations to radiate highly directive wave in space. This type of arrangement is called an array [16, 35]. The overall performance of array configuration depends upon the following parameters:

1. Dimension and geometry of the DRA
2. Spacing between the adjacent elements
3. Number of individual DRA elements used
4. The feeding network
5. Current excitation of individual DRA element, and
6. Phase and radiation pattern of individual DRA element

Various types of arrays are listed below:

1.4.1 Linear array

The number of individual elements when arranged along a single line, as shown in Figure 1.9, is a linear array. The overall radiation pattern is the multiplication of radiation pattern of individual DRA element with its array factor, given by:

Radiation pattern = element factor × array factor

$$E = n \times E_0 \times AF$$

where E is the overall radiated electric field. n is number of individual elements and E_0 is the electric field produced by single DRA at the centre of array at same point. The AF is array factor that depends upon the geometry of array (Linear or Planar), the operating frequency and the phase difference of current among individual elements. The array factor is given by:

$$AF = 1 + e^{j\psi} + e^{j2\psi} + e^{j3\psi} + \cdots + e^{j(N-1)\psi} \tag{1.6}$$

The normalized array factor is given by:

$$AF = \frac{\sin N\psi / 2}{N \sin \psi / 2} \tag{1.7}$$

For array along x-axis direction (Linear E-Plane array), as shown in Figure 1.9(a)

$$\psi_x = \beta S \sin\theta \cos\phi \tag{1.8}$$

For array along y-axis direction (Linear H-Plane array), as shown in Figure 1.9(b)

$$\psi_x = \beta S \sin\theta \cos\phi \tag{1.9}$$

$$\beta = 2\pi / \lambda \tag{1.10}$$

where β is the wave number, λ is the wavelength and S is the distance between the adjacent DRA element.

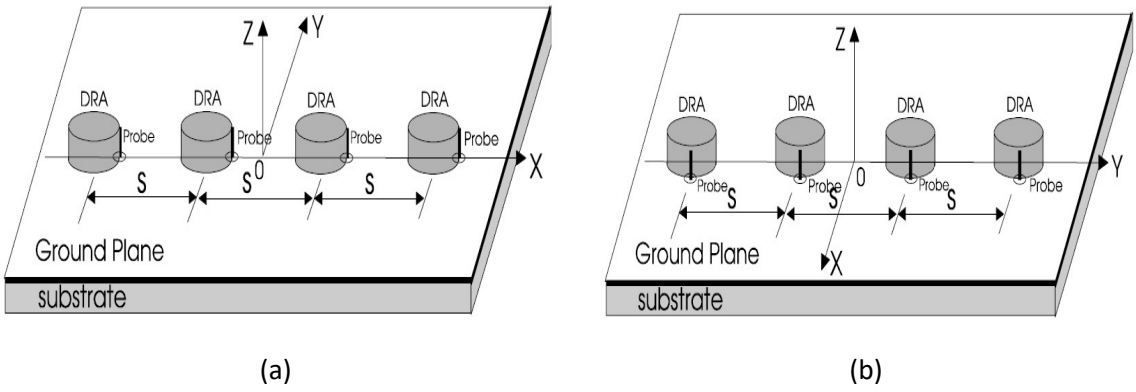

Figure 1.9: The array configuration (a) E-plane along x-axis and (b) H-plane array along y-axis [16].

1.4.2 Planar array

The array factor for planar array is the multiplication of the array factor of the linear array in 2-directions. The planar arrays scan the beam along θ and ϕ, unlike linear array [36]. It offers more gain and lower side-lobe level than the linear array, however more elements are required. The array factor is given by:

$$AF(\theta,\phi) = \frac{1}{NM}\left(\frac{\sin(N\psi_x/2)}{\sin(\psi_x/2)}\right)\left(\frac{\sin(M\psi_y/2)}{\sin(\psi_y/2)}\right) \tag{1.11}$$

$$\psi_x = \beta S_x \sin\theta\cos\phi \tag{1.12}$$

$$\psi_y = \beta S_y \sin\theta\sin\phi \tag{1.13}$$

where S_x and S_y are the distance between the elements along x-direction and y-direction, respectively, as shown in Figure 1.10.

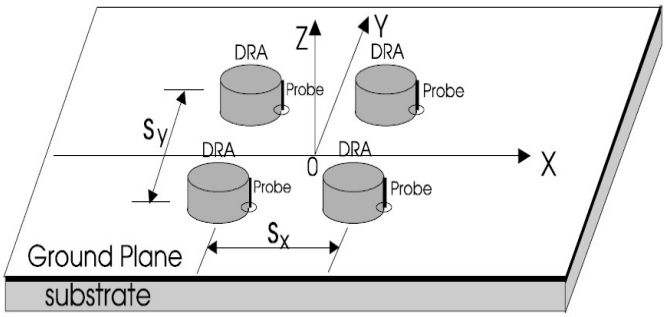

Figure1.10: The planar array configuration [16].

1.4.3 Phased array

The phased array antenna is composed of individual elements arranged in linear or two-dimensional geometry**.** The phase and amplitude excitation of individual element is controlled to radiate the main beam in desired direction. The position of main beam is controlled by electronically adjusting the phase of the individual DRA with fixed antenna aperture [36]. The array factor of the phased array is same as fixed array, accept the overall phase difference occurs due to path difference and individual phase difference and given by

$$\psi_x = \beta S_x \sin\theta\cos\phi - \beta S_x \sin\theta_0 \cos\phi_0 \tag{1.14}$$

$$\psi_y = \beta S_y \sin\theta\sin\phi - \beta S_y \sin\theta_0 \sin\phi_0 \tag{1.15}$$

1.5 Bandwidth enhancement techniques

One of the characteristic of a DRA is its ability to radiate through its whole volume. These volumetric antennas radiate more energy in comparison to the energy stored in the near field. Therefore, the quality factor (Q) factor of these antennas reduces and amount of impedance bandwidth increases. Moreover, the DRA provides wide impedance bandwidth than that of the conventional antennas, which is a key feature for the next generation communication system. There are various bandwidth enhancement methods developed till now [37], and some are listed as follows:

1.5.1 Single element DRA

The DRA is compatible with all the feeding techniques studied for the conventional antennas. Moreover, it is best applicable for higher frequencies due to its low dielectric losses, unlike microstrip antennas. The feeding technique such as microstrip-line, posses a barrier over the functioning of the antenna and produces spurious radiation as the frequency increases. Therefore, the techniques such as aperture feeding, probe feeding, substrate integrated waveguide (SIW), etc, are reported for the higher microwave/millimeter wave frequencies.

However, the SIW feeding experiences narrow bandwidth. Therefore, this feeding technique is loaded with slotted narrow-wall fed high permittivity ϵ_r dielectric loaded substrate integrated cavity (SIC) in co-planar configuration for wide impedance bandwidth and high gain [38]. In this, the cavity modes are analyzed first for the selecting the feeding structure. The PCB technology is used for the fabrication of antenna operating at 35 and 60 GHz bands. For single cavity, the 10% impedance bandwidth with 6dBi gain is obtained for 35 and 60GHz. When this antenna is presented as a 2×2 array at 35GHz, bandwidth of 11.7% with gain up to 10.8 dBi is obtained. The cavity mode and equivalent circuits are analyzed for wideband performance. A half-mode substrate integrated waveguide (HMSIW) is used to feed a CDRA [39]. An aperture slot couples the energy between CDRA and HMSIW. The authors have analyzed this structure for both the linear and circular polarization (CP) by just varying the feeding structure at 60GHz. The rectangular slot and cross slots are used for the linear and circular polarization of the HMSIW, respectively. The authors have analyzed that the former structure exhibits 24.2% bandwidth, ~5.5dB gain with radiation efficiency between 80% and 92% and the later exhibits circular

polarization presenting 3dB axial ratio bandwidth of 4%. These techniques are better for millimeter wave due to compact size, lightweight, wideband and high gain. However the transverse size of posses a major disadvantage.

The bandwidth of the DRA exclusively depends upon the permittivity of the radiating element. Chaudhary et. al. [40] have investigated this by mixing $(Zr_{0.8}\ Sn_{0.2})TiO_4$ with epoxy at five different ratios, i.e., 90:10, 80:20, 70:30, 60:40, 50:50 with a little amount of hardener (HY 951) and found that with increase in epoxy distribution, the complex permittivity of the proposed antenna decreases and bandwidth increases.

1.5.2 Hybrid DRA

The single mode excited DRA do not possess high bandwidth [14]. Using hybrid DRAs multimode gets excited, therefore wideband can be achieved. However, the main challenge of hybrid antennas is to reduce the mutual coupling [41], [42]. The ultra-wideband (UWB) monopole integrated with DRA has been reported to enhance the bandwidth and provide UWB for wireless communication. A hybrid monopole conical and hemispherical dielectric ring resonator (DRR) is presented [43]. The monopole of permittivity 10 is inserted at the center of both the DRRs.. Instead of using cylindrical monopole, a planar monopole is introduced [42] and the authors have integrated a narrow band CDRA with ultra-wideband planar monopole to reduce the mutual coupling and obtained the bandwidth ranging 3.05-11 GHz with voltage standing wave ratio of 2:1. Li et. al. [44] have attached a trapezoidal monopole patch on the DR concave surface as a feeding element for impedance of more than 75% from 2.9GHz to 6.7GHz. However, this prototype is not profitable for terahertz communication due to presence of metal surface.

For the structure to resonate at higher mode with wideband impedance, a multi-layer half-split CDRA fed by the coaxial probe [45]. Each layer of the CDR is having different permittivity and provides an impedance bandwidth of 63.7% from 4.05-6.9GHz and high gain of 5.79 dB. The idea behind the multi-layer structure is that when the DRs are stacked in ascending order of their permittivity, the proposed antennas impedance bandwidth improves. A different feeding structure such a use of bevel shape patch placed beneath the CDRA is designed to enhance the impedance bandwidth [46]. In [47], the authors have proposed a rectangular and cubical DRA with optimum air gap. The proposed antenna is excited by conformal strip and inverted L-shaped microstrip line

feeding. The impedance bandwidth is obtained to be 27.36% at center frequency of 5.78 GHz and 3-dB axial ratio of 23% at center frequency of 5.65 GHz.

1.5.3 Bandwidth enhancement of DRA with dual functioning

Dual functioning antennas are gaining attention due to its innovative features. In case of the planar metallic structures transparent conducting oxides (TCO) films are deployed. However, there is a tradeoff between the electrical conductivity and optical transparency. With increase in transparency the conductivity decreases, therefore lowering the antenna gain and efficiency from there counterpart metallic structures. This problem is solved using the glass DRAs [48]. To validate this concept, Leung et. al. [49] embedded four LED light sources inside omnidirectional hollow rectangular glass DRA. It is observed that the light source have no virtual effect on the performance of the antenna. Later, Leung et. al. [50] modified the former version of the antenna by designing hemispherical DRA to work for WLAN/WiMAX. This DRA is fabricated using K9 glass. The antenna is fed by the slot-coupled radiating at 2.5 and 5.8 GHz. The first band covers both 2.4 GHz WLAN and 2.6 GHz WiMAX and other covers 5.8 GHz WLAN. Instead of using single layer glass DRA, Fang and Leung [51] have investigated two layers transparent HDRA excited in the fundamental omnidirectional TE_{101} mode. The inner and outer layer is made of the acrylic, glass, respectively such that they are used as covering for the LED. As a result, 31.9% impedance bandwidth is obtained using two layer transparent hemispherical DRA, which is twice to a single layer hemispherical DRA (14.2%).

An additional feature of gluing mirror with dual function glass DRA is also reported [52]. Authors have encapsulated the study of both the broadside and end fire radiation pattern using a mirror integrated DRA. The mirror mounted over the top of the DRA with a very thin light reflecting film coated at its back side. TiO_2 and SiO_2 are used as reflecting film. $TM_{01\delta}$ mode is excited by coaxial probe for the end-fire radiation pattern and $HEM_{11\delta}$ mode is excited by the slot coupled feeding for the broadside radiation.

1.6 Gain enhancement techniques

1.6.1 Single element DRA

According to the free space equation, the receiver power is proportional to the transmit power and gain of the transmit antenna and inversely proportional to the square of frequency and distance. At high frequencies it is reported that the transmit power is not sufficient for a stable communication. So the best way to increase the receiver power is to enhance the gain\directivity of the designed antenna. There are various methods to enhance the gain and are listed as follows

By using the additional materials the gain can be enhanced. An infinity shaped metamaterial superstrate is placed over a probe-fed dual segment CDRA [53]. Teflon of ϵ_r=2.1 is used as lower segment and ceramic material of ϵ_r = 22 is referred as upper segment of the radiator. The proposed antenna with or without metamaterial offers experimental peak gain of 12.5 dB at 8.75 GHz and 6.15 dB at 10 GHz, respectively. Kianinejad et al [54] have used a spoof Plasmon (SP) based slow-wave feeding configuration to excite the fundamental TE_{01} mode. Spoof plasmon helps in the excitation of the unusual modes with high isolation providing high gain.

In [55], the authors proposed a photoresist based artificial dielectric with tall embedded metal grids. It is seen that the embedded metal grid boosts the effective permittivity of this material having low permittivity, because of the induction of embedded metal grids. Two new noble model get excited which are different from conventional DRA and a change in the field inside the resonator happens. The resonance is observed at 17GHz and 19GHz with 7.6 and 6.6 dB broad side gain, respectively.

The geometry of any antenna decides its radiation characteristics [56]. In [57], a hollow CDRA of low permittivity is placed above the ground plane. The spherical cap lens and metal reflector is inserted on the top of the CDRA and excited by co-axial probe, making it a mushroom shaped DRA. The suitable shape of spherical cap lens helps in the enhancement of the gain and improves radiation pattern and stability. With the introduction of reflector not only the gain increases but there is reduction of backscattering phenomenon. It produces a broadside radiation pattern and a high gain of 14dBi with fractional bandwidth of 65%. The antenna exhibits excellent efficiency characteristics when either linearly or circularly polarized. Wang et al [58] have obtained a 26% wide bandwidth from 5.4 to 7 GHz due to the stacked structure and high gain of 11 dBi due to the

cavity created by metallic cylinder with a very less VSWR (< 2) using a metallic dielectric and 3 cylindrical DRs made of different material and shapes.

1.6.2 DRA Array:

The other technique to enhance the gain is by combining the gain of various single elements into one. This is performed using array. Gangwar et al [59], have proposed 4 elements RDRA for 5 GHz WLAN/WiMAX band. Its radiation characteristics and specific absorption rate (SAR) in a homogeneous medium for different antenna to muscle layer spacing at 4.9-5.9 GHz frequencies is being presented. It is inferred that bandwidth is 35.25%, which is much wider than single rectangular element. It provides wide angular coverage of 10dB with end-fire radiation. However, for wireless communication broadside radiation is mostly preferred because end-fire provides low radiation gain and narrow bidirectional beamwidth in comparison to former. A half hemispherical DRA with an array of slots is used to increase the gain [60]. Enhanced gain with diversity of the radiation pattern reported using 4 element DRA array [61]. The bandwidth of 700 MHz is obtained ranging from 1.6-2.3GHz. This antenna operates at 4 different modes and therefore, azimuthal variation is checked at Φ=0˚, 90˚, 180˚ and 270˚, keeping θ constant to 45˚.

The study of DRA array is performed at optical frequencies as well. A uniform array of nano scale DR is mounted over a metallic substrate [62]. When normal plane wave in incident, the DR resonates as horizontal magnetic dipole and localized plasmonic are generated. The local plasmonic couples the incident wave bidirectional to the surface plasmon forming standing waves and work as perfect absorber. At 633nm the wave gets perfectly absorbed and we get the bandwidth of about 1.8%.Dense dielectric patch antenna can also be used as an array [63], [64].

1.7 Efficiency enhancement techniques

DRA was first conceptualized as a means to minimize the use of conductor on the resonant portion of the antenna so that the radiation efficiency is enhanced. Mongia et al [65] have measured the radiation efficiency of an antenna due to conduction and dielectric losses. The dielectric resonator is directly placed over a metallic plane and radiation efficiency more than 98% is obtained when operated in $HE_{11\delta}$ mode.

A new idea to enhance the efficiency of the DRA is to use Hyugens' surfaces. Decker et al [66] have proposed a highly efficient all-dielectric meta-surfaces using arrays of silicon nano-disks as meta-atoms for NIR frequencies. Authors observed that it is also useful in beam steering, focusing and shaping of the main beam which is the main requirement of the next generation communication. As discussed before high efficiency is mandatory for future communication. Headland et al [67] have used intrinsic silicon as a radiating element for dielectric resonator antenna at terahertz frequency range. Two different array configuration, uniform array and non-uniform array have been used to enhance the efficiency. Both enhances the efficiency and gives moderate bandwidth. These devices have been characterized experimentally using THz time domain spectroscopy

For future communication system with high data rate, high spectrum efficiency is required. MIMO plays a significant role in providing high spectral efficiency. Khan et al [68] have proposed MIMO rectangular DRA fed by two coaxial probe exciting $TE_{\delta 11}$, $TE_{1\delta 1}$ and some higher modes $TE_{\delta 21}$, $TE_{2\delta 1}$. In this the elements are stacked such that the obtained gain is 5.7dBi and 6.61dBi, impedance bandwidth is 9.97% and 8.88% and port isolation is -13dB and -16 dB at 3.6 and 5.2 GHz, respectively. This proposed antenna is suitable for WiMAX/WLAN applications. Moreover, Messaoudene et. al. [69] have proposed a dual band MIMO DRA for LTE applications. Two orthogonal ports are used to excite the single DRA, hence providing 2 bands at 1.9 and 2.7 GHz. In [70], authors have used the single element and 1x3 array DRA as an efficient energy harvester in microwave frequency. The antenna resonates at 5.5 GHz and energy absorption efficiency came to be about 67%.

1.8 Circular polarization

Polarization of the antenna is defined as the wave transmitted or received by the antenna in a particular direction or we can say that the property which describes the relative magnitude and time varying direction of the electric field vector. There are three different types of polarization, that is, linear (LP), elliptical and circular polarization (CP) [35]. However, circular polarization is chosen for communication because the cross-polarization gets reduced in between transmitter and receiver antenna. There are various ways to generate the CP using DRA. These ways can be divided on the basis of different geometrical shapes and the feeding [71]. The feeding can be

done by the different techniques i.e. slot feeding, microstrip line feeding, slot with microstrip excitation feeding and co-planar waveguide feeding.

1.8.1 Different geometrical shapes:

Excitation of the orthogonal modes helps on the generation of CP. By orienting the multi-elements at a particular angle, these modes get excited. S. Fakhte et al [72] have investigated a DRA, in which four rectangular dielectric layers are placed one over the other at an angle of 30˚. The first and the last layer are separated by angle of 90˚. This proposed antenna exhibits the circular polarization over a bandwidth of 6% ranging from 9.55 to 10.15 GHz, having high radiation efficiency of 93%. The disadvantage of this antenna is if the antenna is not placed at the given angle the cross-polarization can occur. A CP stair-shaped DRA is designed by using two RDRA together combined to form a stair-shaped DRA with a wideband CP radiation [73]. In this antenna, the excitation of multiple orthogonal modes takes place which leads to wide CP bandwidth. The inverted trapezoidal feed is used for wideband CP operation. The antenna has 3 dB axial bandwidth of 22% (5.2-6.5GHz) and impedance bandwidth of 37% (4.6-6.7 GHz) and peak gain of 5.7dB. The radiation efficiency of antenna is more than 90%.

CP is also obtained by changing the antennas physical dimensions. By truncating the corners, the degenerated modes are generated for CP and diagonal slits are introduced for tuning the upper band axial ratio [74-76].

1.8.2 Slot fed DRA:

It is difficult to obtain a dual band CP with good axial ratio for single DRA as compared to the hybrid DRAs, however Zhang et al [77] have examined a cross slot coupled wide dual band CP-RDRA with an impressive axial ratio of 19.8% for lower band and 6.2% for upper band. In the proposed antenna, a cross slot of unequal arms is taken so that the three set of unequal degenerated orthogonal modes TE_{111}, TE_{121}, TE_{131} gets excited and generates dual band CP fields.

For dual polarization a good isolation between the two is required. Four similar bowtie slots are presented to feed the RDRA and measures 40dB port isolation [78]. The symmetrical slots are unconnected and are of cross configuration. This leads to the isolation between two polarizations to improve. This proposed antenna extracts 28-30% of bandwidth with 5-6.4dBi gain. In [79], the

authors have used a simple technique of slot couple feeding to excite dual-band CP RDRA. The TE_{111} and TE_{113} are being excited.

1.8.3 Microstrip fed DRA:

In [80] authors have proposed a wideband CP cubic DRA excited by a question mark shaped microstrip feeding. This provides two orthogonal quadrature phase difference modes which generates circular polarization, offering 35.25% -10dB impedance bandwidth at 3.14GHz and 20.62% 3dB axial ratio bandwidth. The maximum gain came out to be 1.51dB and radiation efficiency of 90.65%. In [81] authors have proposed an omnidirectional cylindrical DRA with horizontal and vertical polarization with low cross coupling. Horizontal polarized radiation pattern is obtained by exciting $TE_{01\delta}$ mode with an 7.4% increased impedance bandwidth by suing air gap and double microstrip feeding arcs whereas vertical polarized radiation pattern is obtained by exciting $TM_{01\delta}$ mode. Good diversity is obtained between 3.78GHz to 4.07GHz. In [82] authors have proposed a high gain 2x2 circularly polarized DRA array with helical exciter. The maximum gain of 13.8dBi is obtained at the operating frequency of 5.2 GHz and CP occurs due to the use of helical exciter in the DRA array structure.

1.8.4 Slot with microstrip fed DRA:

In [83], authors have proposed a combination of microstrip line and aperture slot fed for feeding CP-RDRA. The 3-dB axial ratio is 16.52% and impedance bandwidth is 17.87%. 4.69dB and 74.84% of gain and radiation efficiency is obtained, respectively. A bowtie-shaped DRA with CP is fed by the asymmetric cross-shaped slot which is driven by the microstrip line feeding [84]. The 3 dB axial ratio bandwidth is 7.4% and impedance bandwidth of 43.8%. In [85] authors have proposed a dual-/wide-band CDRA with LP/CP. In this HEM_{111} and HEM_{113} modes are excited to design dual mode CDRA. By merging both the modes, a wide band antenna is obtained. For this antenna a new formula is made by using covariance matrix adaptation evolutionary strategy, which is used to determine the dimensions of CDRA. The effect of varying the two resonant frequencies HEM_{111} and HEM_{113} are considered f1 and f2, respectively. If f2 is fixed and f1 is varying a larger effect is observed on radius than on height and if f1 is fixed and f2 is varying then a larger effect is observed on radius then on height. For dual band design, rectangular slot is introduced in the ground plane to improve matching. DCS and WLAN bands are entirely covered by dualband LP/CP DRA and WiMAX band is entirely covered by wideband LP/CP DRA.

1.8.5 Co-planar waveguide fed DRA:

In [86], authors have proposed a half split 2 layer CDRA with different permittivity in radial direction. CPW feeding is given and $TM_{11\delta}$ mode is being excited for circular polarization. The authors obtained an impedance bandwidth of 25.94% at center frequency of 4.70 GHz and axial ratio bandwidth of 17.34%. The gain and radiation efficiency of 1.56dBi and 93.43% is obtained.

1.8.6 Multi-point fed DRA:

Wilkinson power divider (WPD) and 90˚ phase shifter provides good impedance matching, equal power splitting and 90˚ phase shift which helps in generation of CP. Hang et al [87] have used dual feeding with WPD to obtain a good matched impedance bandwidth over a circularly polarized RDRA. The obtained impedance bandwidth is 50.8% with 3-dB axial ratio of 41.7% and 3-dB gain bandwidth of 45.5% in C-band. Sun and Chen [88] have also used WPD and 90˚ phase shifter for a quadrature fed CP-DRA. The impedance bandwidth of 43.3% (4.7 to 7.3 GHz) at 6 GHz center frequency, axial ratio bandwidth of 42.8% and 3 dB gain bandwidth of 40.8% (4.95 to 7.4 GHz) is obtained. However, to enhance the impedance bandwidth and AR bandwidth then the above given techniques, Sun [89] has proposed a circularly polarized CDRA fed by a dual probe feeding wideband hybrid coupler (WHC). A good impedance bandwidth with high impedance matching can be achieved by using WHC. WPD and a wideband 90˚ phase shifter are embedded in this feed network delivering good impedance bandwidth and equal power splitting.

Similarly switched line coupler also contains WPD and phase shifter for dual fed RDRA design for CP [90]. This coupler gives good impedance matching, equal power splitting and 90˚ phase shift. The axial bandwidth and impedance bandwidth is obtained to be 47.69% and 48.46%.

1.9 Reconfigurable dielectric resonator antenna

With the increase in the demand for good quality communication network and high performance, significant changes are required in the antenna designs. For next generation communication, the concept of reconfiguration is essential so that with changing system requirements these antennas can adapt themselves and increase the antennas performance [95]. Reconfiguration means change in the current distribution inside the radiator that is the electromagnetic fields changes resulting in the change in the radiation properties and impedance of the antenna [35]. Reconfiguration can be

performed on the basis of frequency response [91],[92], radiation pattern [93],[94] and polarization [95],[96]. It can also be performed by changing the material, such as array [97] liquid crystals. Here we will discuss about the frequency reconfiguration. In [98], frequency reconfiguration/tuning is classified into discrete tuning and continuous tuning. In discrete tuning, antenna is able to attain finite number of operating frequencies, whereas in continuous tuning the operating frequency is achieved within the tuning range. This tuning range (TR) is given by: TR $= 2\,\frac{fhigh-f\,low}{fhigh+f\,low}\,\times 100\%$, where f_{high} and $f_{low,}$ refers to the upper and lower frequency bounds of operation. A number of mechanisms can be used for either of the two tuning methods. These mechanisms are structural modification, switches, material change, variable reactive loading and inserting air gap and classified as follows:

1.9.1 Structural and mechanical modification:

Structural changes can bring large frequency shifts but the main challenge is to modify the physical design while maintaining all other parameters. Both liquid and solid DRA are liable for these modifications.

1.9.1.1 Liquid DRA:

Features such as liquidity, reconfigurability and transparency helps recommend liquid materials for the antennas. In liquid DRAs, the structure can be modified by varying the quantity of the liquid DR in the antenna. McDonald and Huff [99] have examined two frequencies RDRA using electromagnetically functionalized colloidal dispersion (EFCD) as dielectric material. The reconfiguration of the proposed antenna is performed by varying the height of the liquid. This antenna design maintains the single mode operation, radiation pattern stability and polarization stability over a large percent configuration bandwidth for S band and C band. Barium strontium titanate is used as the colloidal solution [100] and reconfiguration in this DRA is performed by vertical displacement of columnar fluidic colloidal dispersion. Dispersion of the colloidal is completed in hydrotreated naphthenic oil where the dielectric material is placed in a polycarbonate tube over an aluminum ground plane, which results in a matched impedance bandwidth and throughput. The operating frequencies for the design are in between 2.5 and 4.5 GHz. The coaxial feeding is given for tunable impedance properties. Water, a special liquid has an advantage of accessibility and low cost. The water can be used for reconfiguration at 50 to

100MHz [101]. For higher frequency tuning, Zou et al [102] have proposed an antenna in which water is contained in an acrylic box. Again the height of the water resonator is changed for reconfiguration. A wide tuning frequency range in between 165MHz and 700MHz is obtained. The radiation efficiency of 75% is obtained and can achieve higher efficiency of 90% if the dimension of the design is enlarged at lower frequency.

1.9.1.2 Solid DRA:

The main limitation related to the liquid DRA is the requirement of reservoir as an extra element for varying the quantity of liquid. In these antennas, mechanical loading of the liquid is the only solution. This makes these antennas less feasible for wireless communication. Therefore, solid state antennas are more practical approach. Shaik et al [103] have designed a bandwidth reconfigurable cylindrical DRRA with metallic loading on the outer surface of CDRRA fed by coaxial probe. By varying the height of the metallic loading on outer surface of the CDRRA, there is a considerable shift of upper cut-off frequency (8.2-15.9GHz) and have a controllable bandwidth.

The effective design of the antenna can also be changed with enhanced gain by including the effects of the other materials such as metamaterial and frequency selective surface [104]. Metamaterial structure is used for reconfiguration of two stacked cylindrical dielectric resonator antenna with different dielectric permittivity and radius of 0.32cm and 0.64cm, respectively [105]. Microstrip line feeding is provided and metamaterial structure is used on both side of the feed line to avoid interference in band notching. The UWB response covers a range of 4GHz to 10GHz. Reconfiguration can be achieved by mixing yttrium iron garnet (YIG) with varying amounts of Fe_2O_3 [106].

For next generation communication system gain enhancement is an essential criteria and array or MIMO system is one significant solution [107]. Yan and Bernhard [108] presented a split cylindrical DRA for long term evolution (LTE) femto cell base station. Two modes TE and HE is excited independently with LTE bands 12(698-716MHz, 728-746MHz) and 17(704-716MHz, 734-746MHz). In this the perturbation in the boundary is done so that the amount of energy is stored and resonance frequency changes. The result shows that both the modes resonate at the same frequency of 714MHz and share a common impedance bandwidth. The proposed DRA is

able to achieve 11.1b/s/Hz channels capacity. The proposed method has been verified by both full wave simulation and boundary approximation method.

1.9.1.3 Metallic (parasitic) slots:

The current distribution inside the antenna is changed by inserting the metal slots without modifying the antenna structure. In 1996 Z. Li et al [109] have proposed a cylindrical and ring dielectric resonator antenna. For reconfiguration the diameter of the conducting plate is varied. It is observed that the maximum frequency tuning range reaches to 500MHz from 300MHz. According to Petosa and Thirakoune [110], the current is redistributed by adjusting the shorting tabs on the metallic side wall of the DRA. The authors investigated that this antenna is tuned in between 3.2 and 5.8GHz.

The metallic slots can also be inserted in the ground for frequency tuning. Huang [111] has tuned the DRA by varying the length of the pair of narrow slots in the ground plane. It provides a bandwidth of 3.3% and 3.5% at 1900MHz and 1823 MHz resonant frequencies, respectively. Further, Huang and Ling [112] have embedded two pair of unequal slot on the ground plane. The authors studied that by varying the length of the slot, the frequency is tuned and results in the excitation of two near degenerate orthogonal modes, which leads to circular polarization. For the proposed design CP bandwidth of 3dB axial ratio is about 2.7% at 2.175 MHz.

The parasitic strips are used for tuning the frequency as well as for widening the bandwidth [113]. So and Leung [114] have investigated that by varying the length and position of the parasitic slot placed over a ground plane under DRA, where DRA is slot fed, the antenna can be frequency tuned. Green's function and method of moment is used to solve unknown slot current. Yan and Bernhard [115] have proposed two port reconfigurable MIMO DRA. By the addition of reconfigurable parasitic slot loadings, frequency tuning is achieved. The operating frequency of each radiating port is individually tuned without affecting the frequency response as the two radiating ports are orthogonal to each other. Here multiple frequency mode and MIMO mode is used. In multi-frequency mode, the antenna ports can switch itself independently in the frequency band of interest. In MIMO mode, antenna is reconfigured into a MIMO antenna to increase the capacity when high data traffic is required. The tuning range of the antenna is 615MHz to 836MHz over a tuning ratio of 30%.

Rather than using a metallic slot a conducting cap is loaded at the top of slot fed hemispherical DRA [116]. In this proposed antenna the size of the loading cap is varied for frequency tuning over 3.52GHz, 3.25GHz and 3.68GHz.

In [117] authors have proposed a hemispherical DRA. In this the frequency tuning is done by the multiple parasitic strips placed over the antenna which is able to produce linear and circular polarization. For LP DRA, the parasitic strips of same length but different angular position are placed symmetrically in pair so that cross polarization is minimized. It produces a tunable frequency range of 3.08-3.80GHz. If a second pair of parasitic strips is used then the range increases to 2.8-4.1GHz and also improves impedance matching. For CP DRA, the parasitic strips are made asymmetric by employing genetic algorithm. A good axial ratio (A<1dB) and impedance matching (S_{11}< -15dB) is obtained in a frequency range of 3.2-4.1GHz.

1.9.1.4 Electronic switching:

The metallic switches are better at low frequencies but as the frequency increases the penetration of EM wave inside the metal decreases leading to more conduction losses, therefore switches such as PIN diode can be used as an alternative for the frequency tuning due to its low loss, low cost, better isolation and ease of modeling with lumped circuits [118]. This is applicable in [119], where instead of shorting tabs[110] PIN diode or varactor diode is used to operate the reconfiguration in between 3-8GHz. Salman et al [120] have proposed a slot fed DRA using surface PIN diode for reconfiguration. The SPIN diode is placed in the center of the feeding set. The reconfiguration is done by switching ON and OFF the SPIN. A high gain of 18dB is obtained.

The impedance bandwidth also varies with the variation in the current distributions. Danesh et. al. [121] have presented a coplanar waveguide (CPW) frequency-reconfigurable RDRA, which is tunable at 3 different frequencies in between 3.45 and 6.77 GHz. Two p-i-n diode switches are used. A rectangular dielectric resonator antenna having permittivity of 15 and fed by a U-shaped microstrip line is proposed [122]. A switch is connected at one arm of microstrip line for changing the states between ON and OFF. Frequency switching is done between 4.12GHz and 8.85GHz. Likewise, HPND-4005 PIN is used as a switching device for the reconfiguration of the RDRA of permittivity 10.2 [123].

Till today DRA has shown good results for various applications such as WiMax, WLAN, Bluetooth, DVB-H etc. Danesh et al [124] have studied DRA for WiMax and WLAN applications. The DRA is fed by a coplanar waveguide and frequency tuning is done at 3 different dual band frequencies. Each rectangular DR having ϵ_r = 10 is mounted on a Taconic substrate. Two PIN diodes are connected on the conducting line of the network. The three bands centered at 2.4-5GHz (ON-ON state), 2.5-5.2 GHz (OFF-ON state) and 3.5- 5.8 GHz (ON-OFF state) are obtained. In [125], the authors have investigated a reconfigurable dielectric resonator antenna for LTE/WWAN and WLAN application having tuning frequency between 1.6 and 2.71GHz. It consists of four identical RDRA having permittivity of 10 each and switching is done by 3 p-i-n diode. The size of the RDRA is 20*36*5.57 mm^3 mounted on a microstrip feedline. Khan et al [126] have proposed a frequency reconfiguration of DRA for DVB-H application UHF (470-702 MHz). The two DRs are stacked over each other with lower DRA having the ϵ_r = 30 and upper ϵ_r = 20. Two metallic patches are used to connect the RF switches to the ground plane. The reconfiguration occurs in between 0.47 GHz to 0.89 GHz.

WPD is a three port device used to divide the power equally in between two ports with equal amplitude, zero phase and high isolation. A DRA array which is aperture coupled by WPD is proposed [127]. The reconfiguration is achieved by varying the stub length by switching the two PIN diodes ON/OFF.

1.9.1.5 Variable reactive loading:

Hao et al [128] have investigated a differentially fed dielectric resonator antenna for frequency reconfiguration. The reverse voltage is supplied to different varactors or capacitors loaded on the proposed antenna, so that it can operate at different resonating frequencies discretely or continuously. When capacitive loading is considered, the antenna resonates at different frequencies. The frequency tuning range decreases from 1.98GHz to 1.77GHz as the capacitor value increases from 0pF to 2pF. Further Hao et al [129] have differentially fed the DRA and loaded with chip capacitor or chip varactor for frequency reconfiguration. The two conducting strips with loading elements are attached to the two opposite walls of DRA. The capacitor loaded DRA is simpler in structure as no biasing is required as compared to varactor loaded DRA. Varactor loaded DRA provides dynamic frequency tuning by varying the reverse bias voltage.

1.9.1.6 Air gap reconfiguration:

Apperley and Okoniewshi [130] have proposed a reconfigurable antenna exploiting the air gap effect. For reconfiguration air filled channels are inserted in between DRA and ground plane. Now by sliding metalized dielectric slugs under the resonator, the resonance frequencies lowers. 24.7% switching range is achieved at operating frequency 21.4GHz (9.7% bandwidth) and 16.7GHz (6.15% bandwidth).

1.10 Problem statement

With the exponentially increasing demand for high performance communication networks and production of mobile devices, significant advances in antenna design are essential in order to meet the future requirements. The unique characteristics of Dielectric Resonator Antennas (DRAs) make them suitable for various applications throughout the spectrum, from microwave frequencies to the optical regime. One important feature of DRAs is their high efficiency when the resonator is realized in low-loss high-permittivity dielectric material which arises from their radiation mechanism being mostly based on displacement currents, and opens the door to efficient device realizations towards higher frequencies where the conductor losses degrade the performance of metallic resonators. In addition to this, others attractive properties of dielectric resonator antennas have been extensively documented such as their high design versatility, wide bandwidth and compact size at microwave frequencies [14]. Further, one of the most prominent properties of DRAs was already prominently identified in the original article [1]: DRAs can be very efficient radiators at the highest frequencies relevant for antenna technologies. In fact, DRAs are basically immune to ohmic losses, which can drastically affect the performance of metallic resonators at millimeter/terahertz wave frequencies. Therefore, the recent developments seem to indicate that the DRAs might be best suited for various niche applications, where their specificity and advantages can be fully expressed.

Till now many research have been done in terahertz frequency for communication with the help of existing technology, such as use of microstrip antenna in terahertz frequency giving high directivity and gain but when beam-steering is desired for next generation communication we need a much wider operating bandwidth and stable radiation pattern which can be provided by a dielectric resonator antenna. With wider bandwidth, the antenna is required to radiate with good

gain\directivity. So gain\directivity enhancement technique such as designing antenna array is necessary. As per the demand of antenna for next generation communication system, phased arrays are essential for beam-steering to make the system less bulky and cost effective. The main objective of this dissertation is as follows.

- To analyze and optimize the structure parameters of the proposed dielectric resonator rod antenna (DRRA) at THz frequency for next generation communication system. Further, the proposed antenna is simulated using a commercial simulator CST Microwave Studio to support the analysis. In addition to this, the frequency downscaling is performed to support the analysis of proposed antenna.
- To enhance the gain and directivity of the proposed DRRA, a phased array assembly of the proposed antenna configuration is analyzed and simulated.
- To enhance the bandwidth of proposed DRRA at THz frequency, the tapering of the radiated source is implemented.
- For the next generation communication application, there is a need of beam-steerable, high gain and large bandwidth antenna assembly. Therefore, a phased array DRRA is designed to satisfy this requirement.

1.11 Organization of the Dissertation

The remainder of the dissertation is organized as follows. In Chapter 2 simple DRRA structure is analyzed with full optimization of the structure parameters. The proposed antenna configuration is simulated using CST Microwave Studio. In addition to this, the frequency down scaled analysis is also performed and simulated to support the analysis at terahertz frequency. Further, an array is constructed and beam-steering is done in Chapter 3 with and without mutual coupling for both DRRA and terahertz frequency to enhance the gain and directivity, and down-scaled frequency 11.2 GHz. In Chapter 4, the proposed DRRA configuration is tapered to enhance the bandwidth and its simulation is performed. Further, its phased array assembly is simulated. Chapter 5. Finally, Chapter 6 concludes the work and recommends the future directions.

CHAPTER-2

ANALYSIS AND DESIGN OF DIELECTRIC RESONATOR ROD ANTENNA

2.1 Introduction

The end users of next generation (5G) mobile communication networks requires a major paradigm shift to fulfill the increasing demand for higher data rates, lower network latencies, better energy efficiency, and reliable ubiquitous connectivity. The global bandwidth scarcity facing wireless carriers has motivated the exploration of the underutilized millimeter/terahertz wave frequency regime of the spectrum for future broadband cellular communication networks. Therefore, the millimeter/terahertz wave technology is the major technological breakthroughs that will bring renaissance to wireless communication networks to fulfill the users demand. The ultra-high bandwidth available at millimeter/terahertz frequencies can effectively employed for short-range wireless access networks in small cells enabling potential users for data backhauling and ultra-high-definition infotainment services. However, the knowledge of wave propagation in densely populated indoor and outdoor environments is vital for the design and operation of future generation cellular networks that use the millimeter/terahertz wave spectrum.

Various realizations of DRAs as single elements or in array configurations at microwave frequencies as reported in [14], have demonstrated the versatility of this type of antennas, which typically combine compactness and wide bandwidth of operation. The unique characteristics of Dielectric Resonator Antennas (DRAs) make them suitable for various applications throughout the spectrum, from microwave frequencies to the optical regime. One important feature of DRAs is their high efficiency when the resonator is realized in low-loss high-permittivity dielectric material which arises from their radiation mechanism being mostly based on displacement currents, and opens the door to efficient device realizations towards higher frequencies where the conductor losses degrade the performance of metallic resonators. Various attractive properties of dielectric resonator antennas have been extensively documented such as their high design versatility, wide bandwidth and compact size [14]. Further, one of the most prominent properties

of DRAs was already prominently identified in the original article [1]: DRAs can be very efficient radiators at the highest frequencies relevant for antenna technologies. In fact, DRAs are basically immune to ohmic losses, which can drastically affect the performance of metallic resonators at millimeter/terahertz wave frequencies. The demonstrated high-efficiency of millimeter-wave DRA in both single-element and array configurations provides the rationale to extend their range of applications in the terahertz regime of the spectrum, i.e. at frequencies from roughly 100 GHz to 10 THz [2]. In the next section various related work and problem formulation is presented.

2.2 Related work

The work in the field of optical frequencies has been done for decades. Malherios-Silveria et. al. [131] have examined a nano dielectric resonator antenna for nanophotonic applications. NDRA exhibits an efficient result of high bandwidth and gain and is used efficiently to couple the optical energy into plasmonic circuits. Zou et al [132] have proposed a reflect array based NDRA operating at it fundamental mode at free space visible light. A non uniform array composed of TiO_2 based cylindrical DR is used, introducing a phase delay to the wavefront at resonance, resulting in clearly observable beam deflection at around 633nm. Rather than using the fundamental mode, the reflection mode is chosen [133] and dielectric nanocylinder is mounted over the metal plate. The field distribution, scaling behavior and efficiency of the DRA are studied from microwave to visual frequency band (λ_o from 0.3m to 500nm). In this authors have studied about the high efficiency DRA and reflection metasurfaces at optical frequencies and observed that in Terahertz, the diameter DR is reduced by one third of the value from direct scaling. The efficiency of 90% is achieved from microwave to far-infrared region for DRA. At microwave range, the penetration of EM inside Silver is very less, therefore less conduction losses occur. As the frequency increases toward the visible region, the conductive losses occur in Silver as the field starts to penetrate inside the metal. Author observed that below 1μm, the efficiency drops but DRA is much better approach than patch antenna. Therefore, we can say that the DRA is a promising candidate in terahertz communications. Saleem et al [134] have investigated two CDRA coupled with sensor excited by the $HEM_{11\delta}$ mode rectangular slot resonating at 94 GHz. The antenna exhibits 3GHz impedance bandwidth with a gain of 7.8 dB

and radiation efficiency of 40%. Further moving to the higher frequencies, Deng et al [135] has designed an on chip 3-D antenna. In this a substrate integrated cavity (SIW) of high gain and high radiation efficiency is backing the on-chip antenna and is designed by using standard 0.13μm SiGe BiCMOS technology. A low permittivity supporter and DR are stacked vertically on the on chip antenna forming a Yagi-like antenna; therefore the gain and radiation efficiency enhances. It is observed that the proposed antenna obtains a peak gain of about 10dB, radiation efficiency of about 80% at 340GHz and impedance bandwidth of 12% from 319-360 GHz. In [136] authors have investigated an integrated circuit antenna in which the rectangular cavity is fabricated inside the 80-μm thick InP substrate. Any substrate mode is eliminated by metal via fence surrounding the cavity. The cavity is sized such that its operational bandwidth is near 280GHz at fundamental resonant mode. The 6-dB matching bandwidth is 20GHz from 266 to 286 GHz, with antenna efficiency more than 25% including mismatch loss over a bandwidth of 36GHz from 260 to 296GHz.

In this chapter, we have proposed and design a 170GHz broadband DRRA operating at its fundamental $HEM_{11\delta}$ (TM_{110}) and excited by the probe. Further, we have simulated the proposed antenna using CST Microwave Studio, a commercial simulator based on the finite integration technique to support the numerical analysis. Moreover, we have also presented simulated results of frequency down scale at 11.3 GHz.

2.3 Parametric analysis of the DRRA

A dielectric resonator rod antenna (DRRA) is designed as shown in Figure 2.1. The DRR radiator of height h, with dielectric permittivity of ϵ_{r1} and radius of a is chosen. This DRR is mounted over an Arlon AD 320 (lossy) substrate of dielectric permittivity of ϵ_{r2} and loss tangent of 0.0038 of dimension $0.880\times0.880\times0.762$ mm^3, which is then placed over a metallic ground plane. The DRRA is excited by a probe of radius a_p and height $h_{p,}$ as shown in Table 2.1.

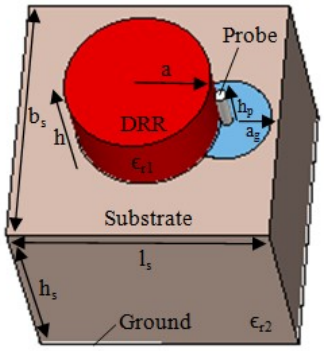

Figure 2.1: Single element DRRA.

Table 2.1: Design parameters of the proposed DRRA.

a (mm)	h (mm)	h_s (mm)	b_s (mm)	l_s (mm)	ϵ_{r1}	ϵ_{r2}	a_p (mm)	h_p (mm)	a_g (mm)
0.245	0.254	0.762	0.88	0.88	8.10	3.20	0.02	1.015	0.125

To yield better impedance matching the height of probe is optimized. The results are simulated using CST Microwave Studio a commercial simulator based on finite integration techniques. We have used the transient solver and the results are supported by the adaptive mesh refinement.

In this the DRRA is excited at its fundamental $HEM_{11\delta}$ (TM_{110}). The probe feeding is employed such that the when located close to the peripheral of the DRA, it yields broadside radiation pattern. The probe is used due to its property of better 50Ω impedance matching and no external feeding network is required. It is observed that the antenna radiates like a horizontal magnetic dipole, exhibiting broadside radiation patterns, low cross-polarization and the largest possible bandwidth (lowest radiation Q-factor) for the cylindrical geometry. The resonance frequency can be determined by the equation [137]:

$$k_o a = \frac{1.6 + 0.513x + 1.392x^2 - 0.575x^3 + 0.088x^4}{\varepsilon_{r1}^{0.42}} \tag{2.1}$$

$$x = \frac{a}{2h} \tag{2.2}$$

$$f_{res}(GHz) = \frac{30k_o a}{2\pi\, a\,(cm)} \tag{2.3}$$

To best estimate the performance of the proposed antenna in real conditions, the frequency of the design is down scaled. In this the frequency is down scaled 15 times so that it analysis is performed at Ka band. The downscaled design resonates at 11.3 GHz. The concept of downscaling arises due to the fact that terahertz devices are not fully developed. Therefore, the analysis at terahertz frequency range becomes difficult. However, if the same proposed antenna when down scaled, gives good results than the proposed design with true structure will be estimated to produce good results. The down scaling of the parameters is given in Table 2.2:

Table 2.2: Frequency Down Scaling

The proposed antenna parameter	**Downscaled parameter**
Radius (a)	a × n
Height (h)	h × n
Frequency (f)	f/n
Permittivity (ϵ)	ϵ
Permeability (μ)	μ
Impedance (Z)	Z
Gain (G)	G

where *n* is the scaling factor and chosen as 15. Therefore, the new dimensions of the frequency down scaled antenna are given in Table 2.3:

Table 2.3: Down scaled parameters for 11.3 GHz.

a (mm)	h (mm)	h_s (mm)	b_s (mm)	l_s (mm)	ϵ_{r1}	ϵ_{r2}	a_p (mm)	h_p (mm)	a_g (mm)
3.675	3.810	11.43	13.2	13.2	8.10	3.20	0.3	15.225	1.875

2.4 Results

The length of probe and diameter of the air gap in between the substrate is chosen arbitrarily to obtain resonance frequency with better antenna performance. The radius of the probe is fixed to 0.02mm. These both parameters are optimized using CST microwave studio 2016. First, the variation of the radius of the air gap is considered by setting the length of the probe 1mm.

The air gap is then fixed to 0.125mm and the length of the probe is changed. It is observed that the probe provides best impedance matching at 0.17THz frequency (S_{11} < -25dB) for 1.015mm length, i.e., length of the probe is optimized to yield better impedance matching. After computing the length of probe, the simulation is performed to yield the S-parameter, gain and efficiency of the proposed antenna. It is observed that the proposed antenna resonates at 0.17THz as well as at 0.227THz frequency and -10dB impedance bandwidth of 79.7 GHz is obtained as shown in Fig. 2.2.

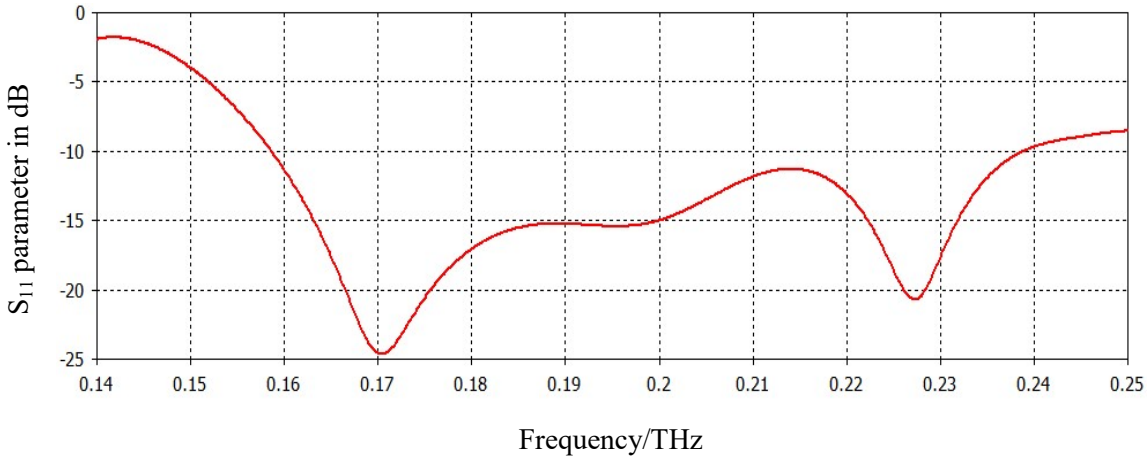

Figure 2.2: S-parameter of the DRRA.

At the 0.17THz operating frequency, the gain, directivity and radiation efficiency are 8.885dB, 8.937dBi and 98%, respectively as shown in Figure 2.3(a). In the E-plane, the proposed antenna shows that the magnitude of main beam is 8.89 dB with its direction at 9°, angular width (dB) of

59.4˚ and side lobe level of -11.1dB. Similarly, in the H-Plane, the proposed antenna shows the main lobe magnitude of 8.61 dB with main lobe direction at 0˚, angular width (dB) 68.1˚, as shown in Fig. 2.3(b).

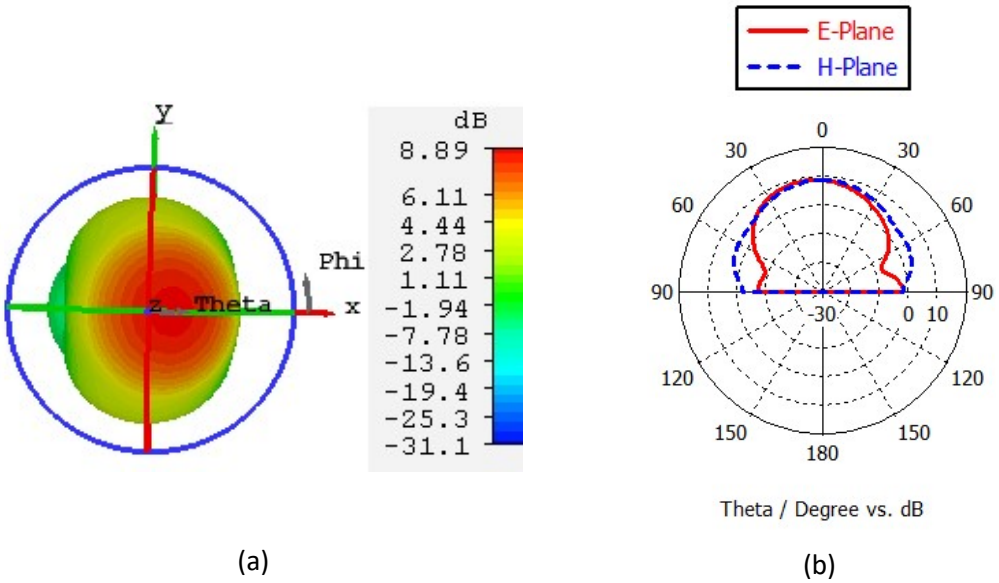

(a) (b)

Figure 2.3 : The radiation characteristics (gain) of the proposed antenna (a) 3D far-field and (b) E-plane and H-Plane at 0.17 THz.

The electric and magnetic field distribution of the proposed DRRA is shown in Figure 2.4. It is observed that this proposed antenna exhibits the fundamental mode $HEM_{11\delta}$ from the two field distribution working as a horizontal magnetic monopole.

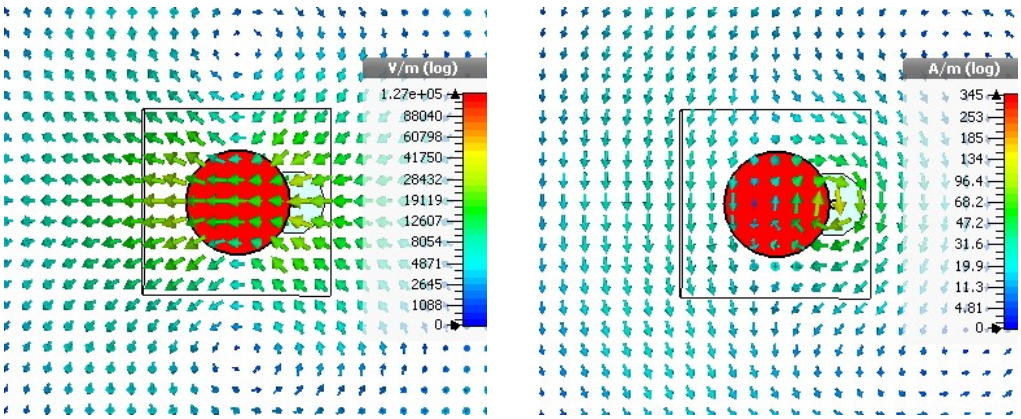

(a) (b)

Figure 2.4: At 0.17THz frequency (a) E-field and (b) H-field distributions.

The current distribution of the proposed antenna is such that the maximum current passes through of the surface of the DRRA, this is shown in Figure 2.5

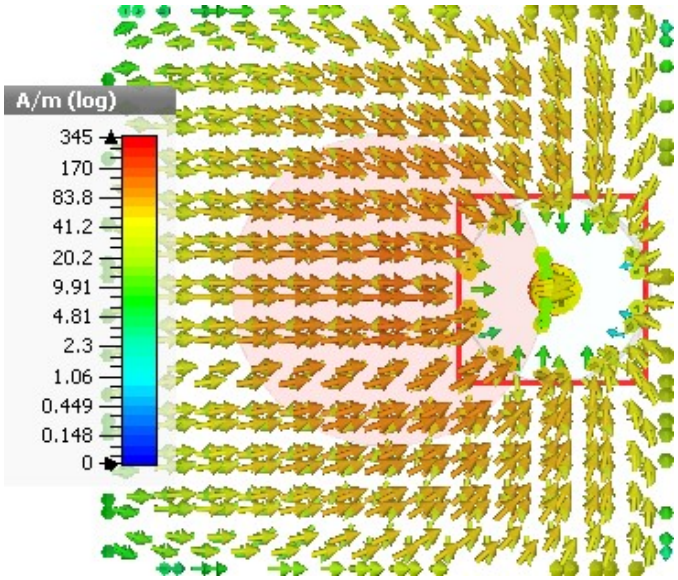

Figure 2.5: The surface current distribution of the proposed DRRA.

After the analysis of the DRRA at 170GHz, the frequency is downscaled to 11.3GHz by a scaling factor of 15. The new design is then measured and simulated using CST microwave studio 2016. This antenna provides a wide bandwidth of 5.3GHz ranging from 10.6 to 15.9 GHz with two resonant peaks. One at 11.3 GHz (S_{11}=-24.39 dB) and other at 15.18 GHz (S_{11}= -20.21 dB).

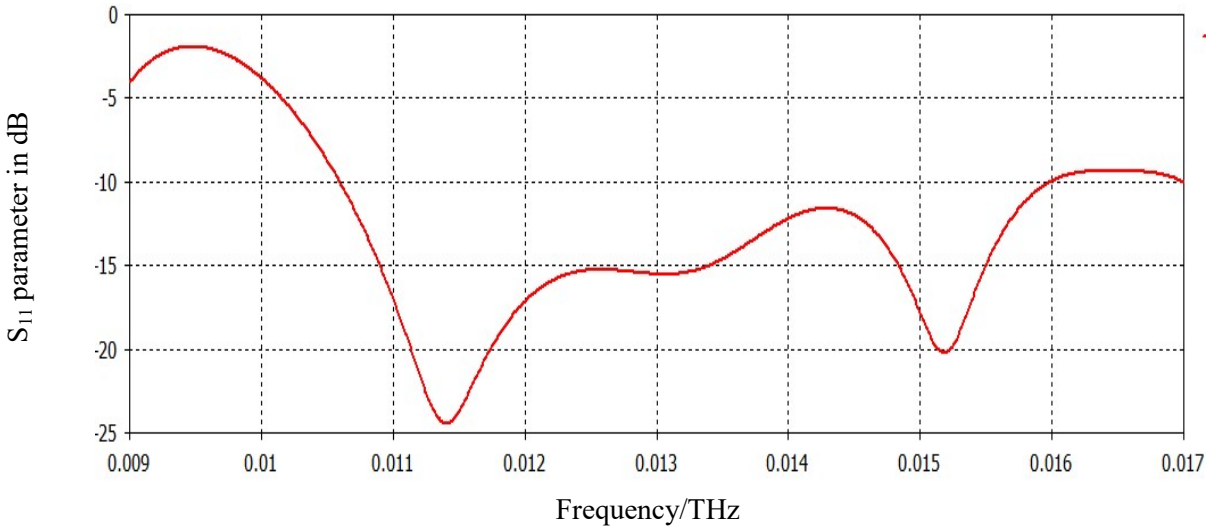

Figure 2.6: S-parameter of the down scaled antenna.

At 11.3 GHz, the directivity and gain of the proposed antenna is 8.033 dBi and 7.97 dB, respectively, with radiation efficiency of 98.5% as shown in Figure 2.7(a). For E-plane, the main lobe magnitude is 7.97 GHz with main lobe direction at 10˚ and 3dB angular width of 67.9˚ whereas in H-plane, the main lobe magnitude is 7.66 GHz with main lobe direction at 0˚ and 3dB angular width of 69.6˚, is shown in Figure 2.7(b).

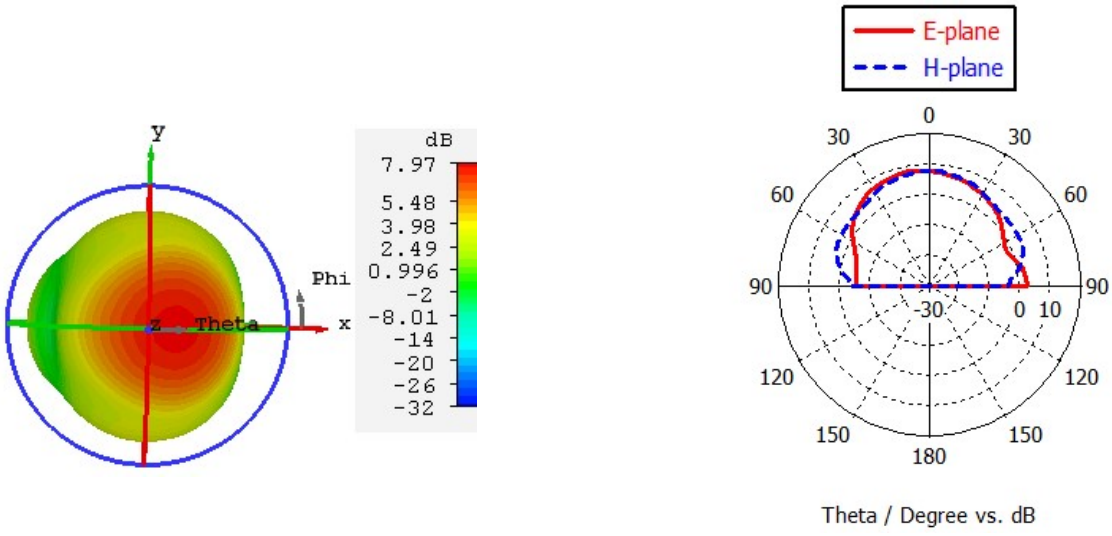

Figure 2.7: The radiation characteristics (gain) of the proposed antenna (a) 3D far-field and (b) E-plane and H-Plane at 11.3 GHz.

2.5 Conclusion

DRA plays a signicant role for next generation terahertz communication by providing wider impedance bandwidth with very low dielectric losses and high efficiency. The parameter analysis of the DRRA is computed for 0.170 THz resonant frequency. A wideband of 79.7 GHz with dual resonance dips are obtained at 0.170 THz and 0.227 THz. At 0.170 THz the gain, directivity and radiation efficiency of 8.885dB, 8.937dBi and 98%, respectively is achieved.

Due to the scarcity of terahertz devices, the concept of frequency downscaling is implemented on DRRA. The frequency is down scaled by a factor of 15 and the downscaled antenna resonates at 11.3GHz with 5.3GHz impedance bandwidth and approximately same gain (7.97 dB). The directivity and efficiency of 8.033dBi and 98%, respectively is obtained. However, the major limitation of the DRRA is that it provides insafficient gain for communication applications. Therefore there is a requirement of implementing design techniques to enhance its gain/directiviy**.**

CHAPTER 3

THE DIELECTRIC ROD RESONATOR ANTENNA PHASED ARRAY

3.1 Introduction

For the future generation communication system the millimeter and terahertz wave frequencies have become an attractive topic among several research groups in recent years, which demand efficient antennas in terms of losses and costs, both in transmission and reception scenarios. A single unit DRA supports wideband communication applications. However, the small gain and directivity of this proposed antenna at terahertz frequencies in comparison to the conventionally used antennas is the major limitation. To enhance the gain and directivity of the DRRA, the array configuration of the proposed is useful for the future generation communication system. At terahertz frequency, the dimension of the antenna becomes smaller therefore a number of single element DRAs can be fabricated to form an array. An array of DRRA antennas can effectively combine the power of an arbitrary large number of terahertz wave sources while keeping cost-affordable and lightweight.

A potential study of the beam steering properties of the array is also performed. For the scanning purpose there is a need to switch the generated beam from the antenna array at a particular angle. Moreover, the beam-steering phenomenon helps to cover a large area with the use of single antenna array assembly. By providing a progressive phase shift to each element of a DRRA array, a high gain beam can easily be switched at different scan angles providing high coverage for the end users.

3.2 Related work

The additional techniques such as surface plasmons, metamaterial and design modifications such as designing an array, reflect array or phased array are best suited for enhancing the antenna parameters to desired level. Headland et al [138] have used intrinsic silicon as a radiating element for dielectric resonator antenna. Two different array configurations, i.e., uniform array and non-

uniform array have been used to enhance the efficiency. In uniform array configuration quality factor is analyzed and unveils that absorption quality factor is greater than radiation quality factor, hence efficiency enhances. The uniform array works as a magnetic mirror and the non-uniform array works as an off-axis focusing reflect array mirror. Both enhances the efficiency and gives moderate bandwidth. These devices have been characterized experimentally using THz time domain spectroscopy.

Moreover to fill the technical gap problem in the terahertz band and to enhance the radiated power, [139] dielectric rod waveguide antenna is proposed with full electronic beam-steering. A 4x4 array is employed at 100GHz. DRW phase shifters are used and the main lobe is steered in one or both the planes. This proposed antenna has higher power level than the lens. In [140] THz emitting is done by dielectric rod waveguide antenna (DRWA) with photomixer. This approach is overwhelming from the classical approach (Si lens) as it is an inexpensive alternative to substrate lens. It helps in the reduction of scattering and reflection of terahertz power into the substrate and the surface. This antenna utilizes the whispering gallery mode resonators through evanescent coupling as excitation. Here the radiation pattern is measured at 137 GHz and has shown the satisfactory performance.

In this chapter, to enhance the gain, the phased array DRRA is implemented using a detailed parametric analysis. Firstly, the far-field of the antenna array is simulated without considering the mutual coupling between the individual elements of the DRRA. Secondly, using Taylor current distribution the far-field of this antenna array is stimulated while considering mutual coupling using combined results of transient solver in CST microwave studio. Further the frequency downscaling is also implemented. The designs are then progressively phase shifted in single axis (x-direction) and in a plane (x-, y-direction).

3.3 Parametric analysis of the DRRA phased array

Sixteen individual elements are combined together as shown in Figure 3.1, to form a planar phased array configuration. The dimension of each element is same and every element is phase shifted independently. The spacing between individual DRRA elements (center to center) is *d*. To

reduce the side-lobe level, the spacing between the element is taken $d=\lambda/2$, where λ is the resonant wavelength of the proposed antenna.

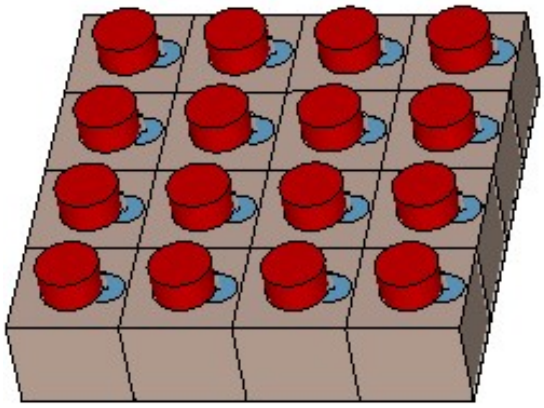

Figure 3.1: 4 x 4 DRRA phased array configurations using single element DRRA.

For the planar phased array configuration, the array factor is the multiple of the linear array factor in *x*-direction and *y*-direction.

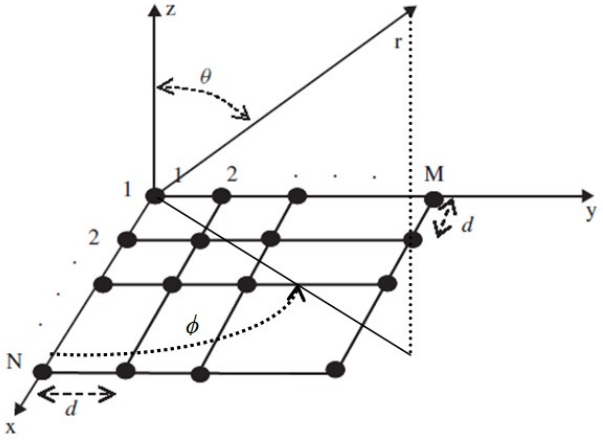

Figure 3.2: M x N rectangular planar array antenna geometry [35]

The far-field pattern is given by the multiplication of the single element factor with the array factor that is why in CST after examining the single antenna element the results are combined to give the far-field pattern. In this we have considered the antenna array in xy-plane and direction of the main beam in z-direction. The mn^{th} element is located at $x=nd_x$ and $y=md_y$, as shown in Figure 3.2. Array factor at both the directions is given by [35]

$$AF_x(\theta,\varphi) = \sum_n a_{xn} \exp jn\psi_x \tag{3.1}$$

$$AF_y(\theta,\varphi) = \sum_m a_{ym} \exp jm\psi_y \tag{3.2}$$

ψ_x, ψ_y, are phase taper. The equations are given by

$$\psi_x = \beta d_x \sin\theta\cos\phi - \beta d_x \sin\theta_0 \cos\phi_0 \tag{3.3}$$

$$\psi_y = \beta d_y \sin\theta\sin\phi - \beta d_y \sin\theta_0 \sin\phi_0 \tag{3.4}$$

$$\beta = 2\pi/\lambda \tag{3.5}$$

$\psi_{x0} = \beta d_x \sin\theta_0 \cos\phi_0$, it is element-to-element progressive phase shift in x-direction. (3.6)

$\psi_{y0} = \beta d_y \sin\theta_0 \sin\phi_0$, it is element-to-element progressive phase shift in y-direction. (3.7)

For uniform spacing, normalized array factor is given by

$$AF(\theta,\phi) = \frac{1}{NM}\left(\frac{\sin(N\psi_x/2)}{\sin(\psi_x/2)}\right)\left(\frac{\sin(M\psi_y/2)}{\sin(\psi_y/2)}\right) \tag{3.8}$$

So for the planar array, the array factor is given by

$$AF(\theta,\phi) = \sum_n \sum_m I_{nm}[\exp j(n\psi_x + m\psi_y)] \tag{3.9}$$

I_{nm} is the amplitude excitation of each element. For the proposed 4x4 DRRA phased array, a planar array is considered, where n=4 and m=4. The distance between each element is taken $\lambda/2$, both for d_x and d_y. Here we have performed the beam-steering in elevation plane and azimuthal variation is kept constant, hence ϕ_0 = 0˚. Therefore, the array factor is given by

$$AF(\theta,\phi) = \sum_4 \sum_4 I_{nm} \exp[j4\pi(\sin\theta\cos\phi - \sin\theta_0) + j4\pi(\sin\theta\sin\phi)]$$

The main beam is then steered by changing the phase of the individual antenna element. Likewise the frequency down scaling is performed and the results are simulated for the new antenna design working at X-band for the estimation of the proposed antenna design.

3.4 Results

The design is measured and then simulated in CST microwave studio. First, the far-field results are realized without any mutual coupling with uniform current distribution. Further the results are obtained while considering the effect of mutual coupling between the elements using Taylor current distribution for both the proposed broadband design and frequency downscaled design. The frequency scanning is performed in single axis (x direction) as well as in a plane (xy-direction).

3.4.1 4×4 DRRA Phased Array Configuration without mutual coupling

For the phased array simulation, a finite full array of 4×4 is constructed. The transient analysis over the design is performed. The main beam of the antenna is steered at $\phi = 0°$ and $0° \le \theta \le 60°$, where the sidelobe level < -10dB is obtained for uniform current distribution. In this, the progressive phase shift is applied along x-axis. The results are obtained for the resonance frequency of 0.17 THz. From Figure 3.3, it is observed that by changing the scan angle, the main beam steers in E-plane, unlike in H-plane where only the magnitude changes. The results for the E-plane and H-plane are shown in Table 3.1 and 3.2, respectively.

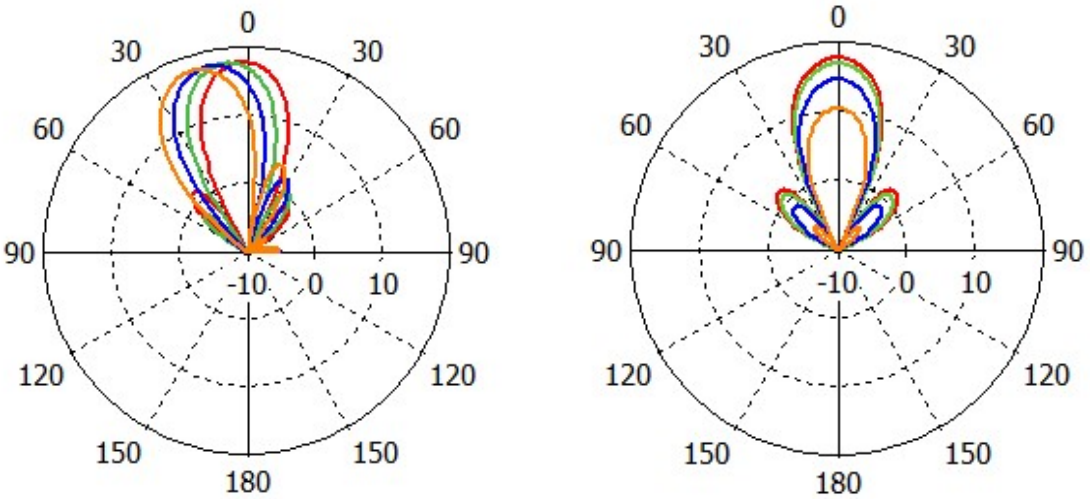

Figure 3.3: Beam-steering at scan angle 0˚(red), 20˚(green), 40˚(blue) and 60˚(orange) for E-Plane (a) and H-Plane (b)

Table 3.1: For E-plane progressive phase shift in x-direction for uniform distribution.

Progressive Phase shift (deg)	Main lobe magnitude (dB)	Main lobe direction (deg)	Angular width (dB)	Side-lobe level (dB)
0	17.8	2	24.3	-16.1
20	17.7	7	24.4	-17.3
40	17.6	12	24.6	-15.7
60	17.4	18	24.8	-14.1

Table 3.2: For H-plane progressive phase shift in x-direction for uniform distribution.

Progressive Phase shift (deg)	Main lobe magnitude (dB)	Main lobe direction (deg)	Angular width (dB)	Side-lobe level (dB)
0	17.7	0	24.6	-16
20	16.9	0	24.6	-16
40	14.7	0	24.6	-16
60	10.4	0	24.6	-16

It is observed that for E-plane with every 20˚ phase shift the main lobe direction changes by approximately 5˚, whereas for the H-plane the main lobe direction remains 0˚. Then, the progressive phase shift is applied in the xy-plane (both the directions). The simulated results are shown in Figure 3.4 and Table 3.3 and 3.4.

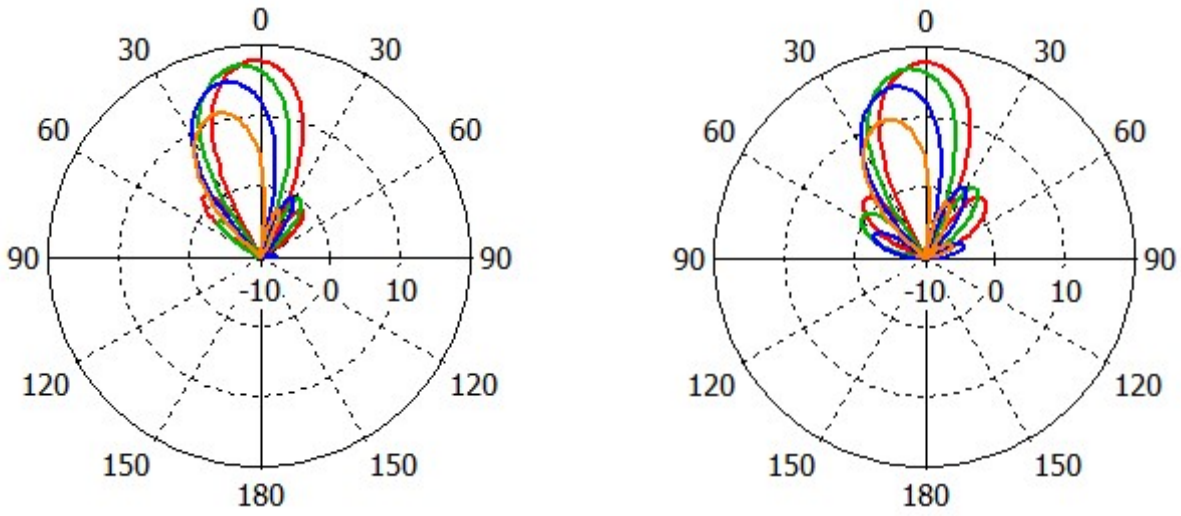

Figure 3.4: Beam-steering at angle 0˚(red), 20˚(green), 40˚(blue), 60˚(orange) at (a) E-Plane and (b) H-Plane.

Table 3.3: For E-plane progressive phase shift in xy-plane for uniform distribution.

Progressive Phase shift (deg)	Main lobe magnitude (dB)	Main lobe direction (deg)	Angular width (dB)	Side-lobe level (dB)
0	17.8	2	24.3	-16.1
20	17.2	7	24.4	-17.3
40	15.2	12	24.6	-15.7
60	11.2	18	24.8	-14.1

Table 3.4: For H-plane progressive phase shift in xy-plane for uniform distribution.

Progressive Phase shift (deg)	Main lobe magnitude (dB)	Main lobe direction (deg)	Angular width (dB)	Side-lobe level (dB)
0	17.7	0	24.6	-16
20	16.9	5	24.7	-14.7
40	14.6	11	24.9	-13.3
60	10.4	17	25.2	-11.8

It is observed that for both E-plane and H-Plane with every 20˚ phase shift the main lobe direction changes by approximately 5˚ with side-lobe level <-10dB.

3.4.2 4×4 DRRA Phased Array Configuration with mutual coupling using Taylor current distribution

The main limitation with the CST far-field simulation is it does not consider the mutual coupling in between the elements. Mutual coupling results in the variation of the radiation pattern of the antenna and degrades the performance if it is high. Therefore, it is a necessity to minimize the mutual coupling. Moreover, the reduction of the relative side-lobe level is also required and for this the Taylor current distribution is provided to each element of the antenna array because the uniform current distribution was not giving satisfactory results. The simulated results for progressive phase shift in x-axis are shown in Figure 3.5 and Table 3.5 and 3.6.

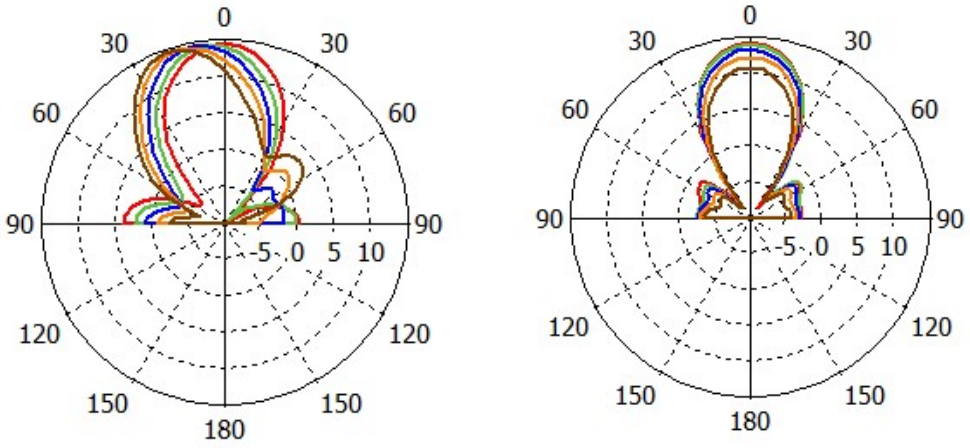

Figure 3.5: Beam-steering at angle 0˚(red), 10˚(green), 20˚(blue), 30˚(orange) and 40˚(brown) at (a) E-Plane and (b) H-Plane

Table 3.5: For E-plane progressive phase shift in x-direction for Taylor distribution.

Progressive Phase shift (deg)	Main lobe magnitude (dB)	Main lobe direction (deg)	Angular width (dB)	Side-lobe level (dB)
0	14.4	0	35.4	-10.7
10	14.3	5	35.2	-12.1
20	14.3	10	34.5	-13.5
30	14.5	15	33	-13.5
40	14.6	20	31.3	-11.3

Table 3.6: For H-plane progressive phase shift in x-direction for Taylor distribution.

Progressive Phase shift (deg)	Main lobe magnitude (dB)	Main lobe direction (deg)	Angular width (dB)	Side-lobe level (dB)
0	14.2	0	34	-15.8
10	14	0	34	-15.7
20	13.3	0	34	-15.7
30	12.2	0	34	-15.3
40	10.7	0	34.1	-14.4

When the progressive phase shift is applied in x-direction for $0° \le \theta \le 40°$ keeping $\phi = 0°$, the relative side-lobe level remains less than -10 dB. However while considering the mutual coupling, the main beam gain is less than the gain obtained without mutual coupling and due to this the angular width also increases. Moreover, here with every 10˚ phase shift there is shift of 5˚ of the main lobe unlike uniform distribution without coupling.Now for the Taylor distribution, the phase shift is applied in both the directions, as shown in Figure 3.6. It is observed that the magnitude of the main lobe decreases due to the impedance mismatch as the beam gets shifted at different angles. The simulated results are shown in Table 3.7 and 3.8.

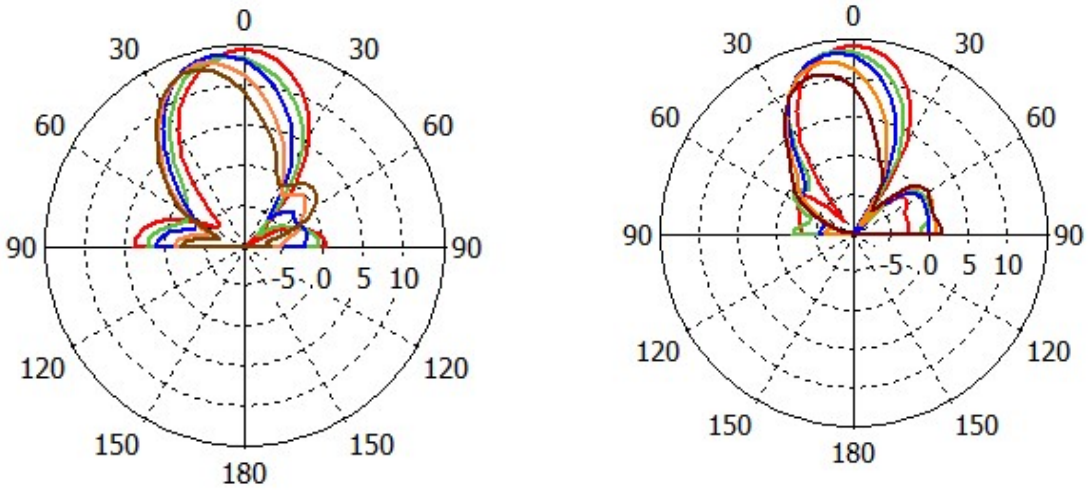

(a) (b)

Figure 3.6: Beam-steering at angle 0˚(red), 10˚(green), 20˚(blue), 30˚(orange) and 40˚(brown) at (a) E-Plane and (b) H-Plane

Table 3.7: For E-plane progressive phase shift in xy-plane for Taylor distribution.

Progressive Phase shift (deg)	Main lobe magnitude (dB)	Main lobe direction (deg)	Angular width (dB)	Side-lobe level (dB)
0	14.4	0	35.4	-10.7
10	13.7	5	37.4	-11.6
20	14	10	34.7	-12.9
30	13.3	15	32.8	-13.7
40	12.7	20	31	-11.5

Table 3.8: For H-plane progressive phase shift in xy-plane for Taylor distribution.

Progressive Phase shift (deg)	Main lobe magnitude (dB)	Main lobe direction (deg)	Angular width (dB)	Side-lobe level (dB)
0	14.2	0	34	-15.8
10	13.6	5	35.5	-13.1
20	13.3	5	33.1	-13.4
30	12.4	10	31.4	-11.4
40	11.1	15	30.5	-9.6

It is observed that the for every 10˚ phase shift in xy-plane, the main beam gets shifted by 5˚ for both E-plane and H-plane.

3.4.3 4×4 DRRA Phased Array Configuration without mutual coupling using uniform distribution for frequency downscaled design

It is required that the frequency downscaled design should provide same gain as that of the proposed antenna. So the new design at 11.3 GHz is simulated and observations are reported in Figure 3.7 and Table 3.9 and 3.10.

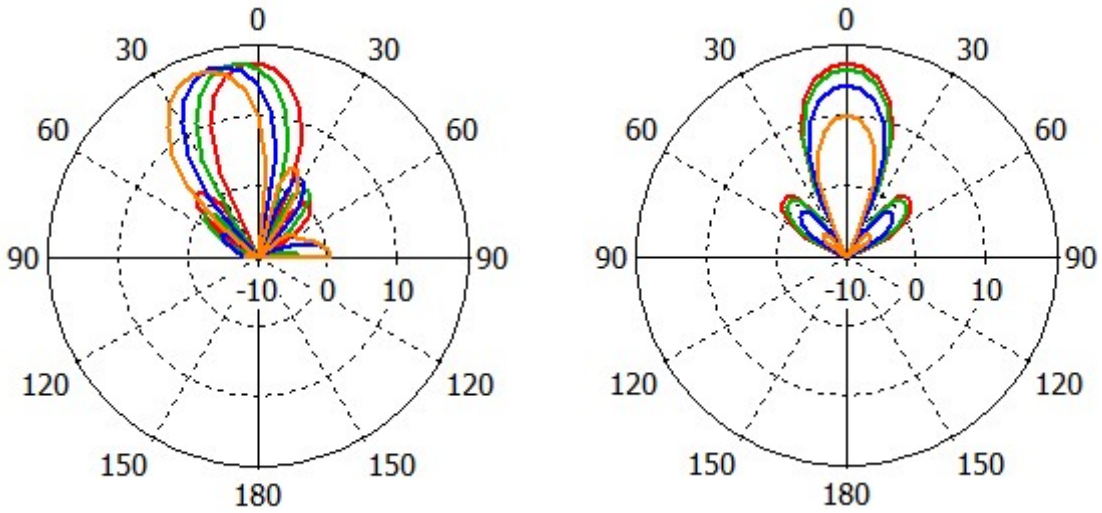

Figure 3.7: Beam-steering at angle 0˚(red), 20˚(green), 40˚(blue), 60˚(orange) at (a) E-Plane and (b) H-Plane.

Table 3.9: For E-plane progressive phase shift in x-direction for uniform distribution.

Progressive Phase shift (deg)	Main lobe magnitude (dB)	Main lobe direction (deg)	Angular width (dB)	Side-lobe level (dB)
0	17.5	0	24.6	-15.1
20	17.5	5	25	-15.7
40	17.4	10	25.1	-14.6
60	17.4	20	25.2	-13.8

Table 3.10: For H-plane progressive phase shift in x-direction for uniform distribution.

Progressive Phase shift (deg)	Main lobe magnitude (dB)	Main lobe direction (deg)	Angular width (dB)	Side-lobe level (dB)
0	17.5	0	24.1	-15.5
20	16.6	0	24.6	-16
40	14.3	0	24.6	-16
60	10	0	24.6	-16

It is observed that the new design provides approximately same result as the desired antenna radiates. For the x-axis phase variation, the beam gets shifted by 5˚ with every 20˚ shift in the scan angle. Similarly, the results are simulated for scanning in xy-plane. It is depicted in Figure 3.8 and Table 3.11 and 3.12.

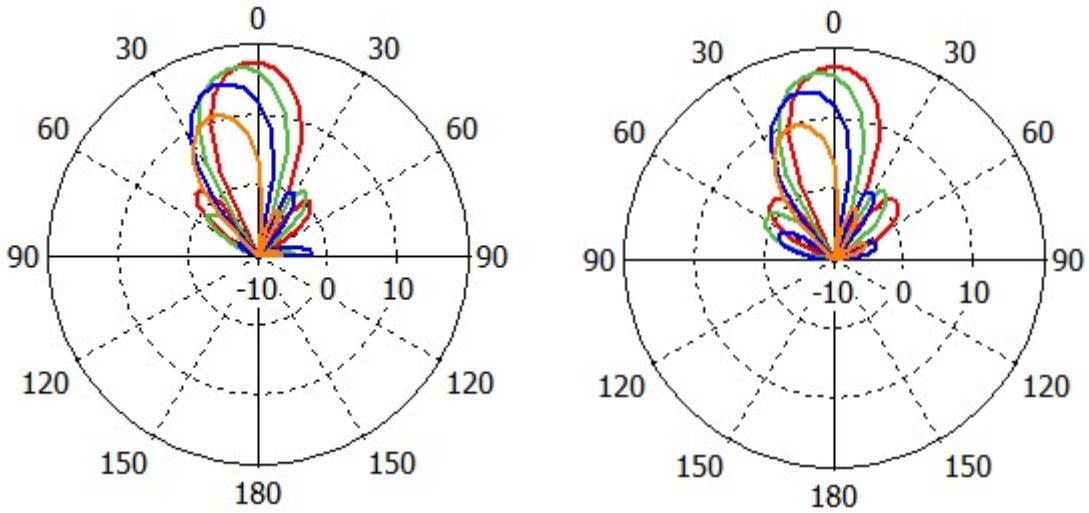

Figure 3.8: Beam-steering at angle 0˚(red), 20˚(green), 40˚(blue), 60˚(orange) at (a) E-Plane and (b) H-Plane.

Table 3.11: For E-plane progressive phase shift in xy-plane for uniform distribution.

Progressive Phase shift (deg)	Main lobe magnitude (dB)	Main lobe direction (deg)	Angular width (dB)	Side-lobe level (dB)
0	17.5	0	24.6	-15.1
20	16.9	5	25	-15.7
40	14.8	15	25.4	-14.6
60	10.7	20	25.2	-13.8

Table 3.12: For H-plane progressive phase shift in xy-plane for uniform distribution.

Progressive Phase shift (deg)	Main lobe magnitude (dB)	Main lobe direction (deg)	Angular width (dB)	Side-lobe level (dB)
0	17.5	0	24.1	-15.5
20	16.6	5	24.2	-14.7
40	14.3	10	24.7	-13.3
60	9.76	15	25.5	-12

3.4.4 4×4 DRRA Phased Array Configuration with mutual coupling using Taylor distribution for frequency downscaled design

The Taylor current distribution is then applied to the new design and the results are shown in Figure 3.9 and Table 3.13 and 3.14 for the progressive phase shift in x-axis.

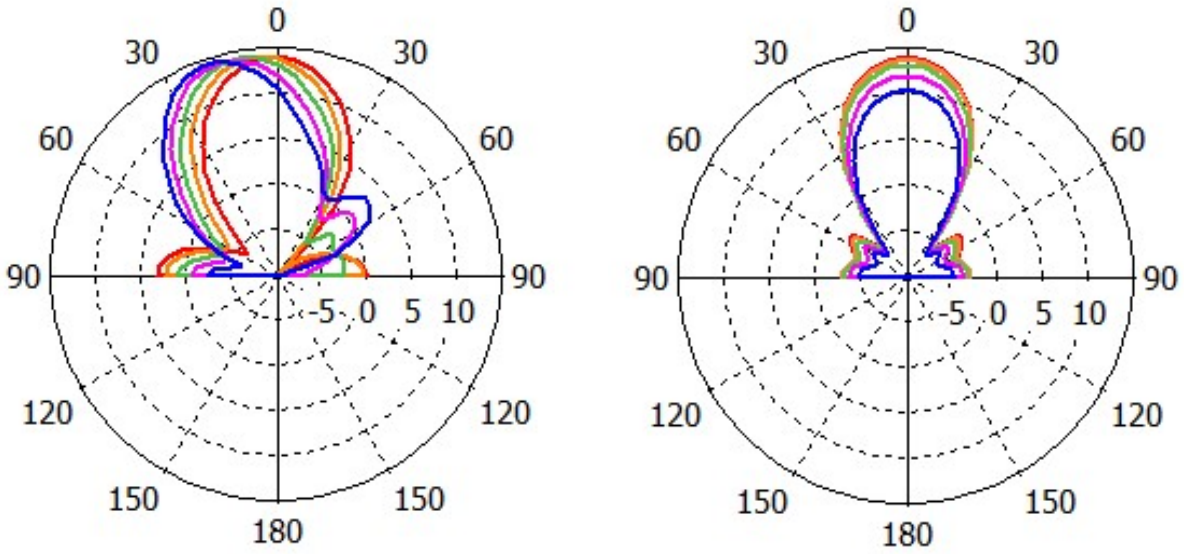

Figure 3.9: Beam-steering at angle 0˚(red), 10˚(orange), 20˚(green), 30˚(pink) and 40˚(blue) at (a) E-Plane and (b) H-Plane.

Table 3.13: For E-plane progressive phase shift in x-direction for Taylor distribution.

Progressive Phase shift (deg)	Main lobe magnitude (dB)	Main lobe direction (deg)	Angular width (dB)	Side-lobe level (dB)
0	14	0	35.5	-10.8
10	14.1	5	35.7	-11.8
20	14.1	10	35.3	-13.2
30	14.3	15	33.8	-13.7
40	14.4	20	31.8	-11.5

Table 3.14: For H-plane progressive phase shift in x-direction for Taylor distribution.

Progressive Phase shift (deg)	Main lobe magnitude (dB)	Main lobe direction (deg)	Angular width (dB)	Side-lobe level (dB)
0	14	0	34.1	-16.5
10	13.8	0	34.1	-16.7
20	13.1	0	34	-16.3
30	12	0	34.1	-15.8
40	10.4	0	34.1	-15.1

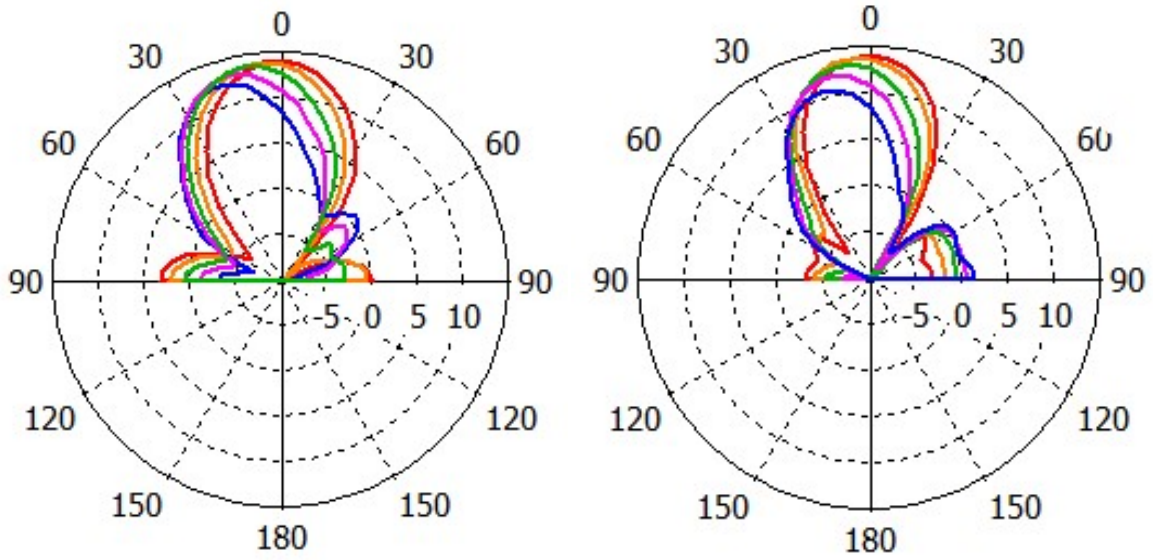

(a) (b)

Figure 3.10: Beam-steering at angle 0˚(red), 10˚(orange), 20˚(green), 30˚(pink) and 40˚(blue) at (a) E-Plane and (b) H-Plane

Similarly, the analysis of the new design is done using Taylor for the scanning in both x-y-directions, as shown in Figure 3.10 and Table 3.15 and 3.16.

Table 3.15: For E-plane progressive phase shift in xy-plane for Taylor distribution.

Progressive Phase shift (deg)	Main lobe magnitude (dB)	Main lobe direction (deg)	Angular width (dB)	Side-lobe level (dB)
0	14	0	35.4	-10.7
10	13.9	5	37.4	-11.6
20	13.6	10	35.1	-12.9
30	13.1	15	33.6	-14
40	13.9	20	31.4	-11.7

Table 3.16: For H-plane progressive phase shift in xy-plane for Taylor distribution.

Progressive Phase shift (deg)	Main lobe magnitude (dB)	Main lobe direction (deg)	Angular width (dB)	Side-lobe level (dB)
0	14	0	34.1	-16.5
10	13.8	5	34	-15.6
20	13.1	5	33.4	-13.7
30	12.2	10	32	-11.7
40	10.8	15	31.2	-9.6

3.5 Conclusion

High antenna gain/directivity is essential for long distance communication. In this chapter, the concept of beam-forming by a phased array is introduced for a wideband DRRA operating at 0.170 THz. The array configuration helps enhancing the gain of the system, therefore a 4×4 phased array design is implemented. The phased array when considered without the mutual coupling between the elements provides a high gain for the progressive scanning in single axis or a plane for uniform current distribution. . It is found that this proposed antenna works for the scan angle of $0° < \theta < 60°$ and $\varphi = 0°$ such that side-lobe level is less than -10dB. For the scan in x-direction the beam is steered by 5˚ in E-plane whereas only the magnitude changes in the H-plane for every 20˚ phase shift and while scanning in the xy-direction, the beam is steered in both the

planes by 5˚. However, the magnitude of the beam decreases for every 20˚ scanning due to impedance mismatching. This design is then evaluated with mutual coupling using Taylor distribution. Similar analytical procedure is followed, i.e., scanning the beam in single axis and a plane. Here for every 10˚ phase shift, the main beam shifts by approximately 5˚ for E-plane when scanned in x-axis (magnitude changes in H-plane) and for both E-plane and H-plane when scanned in the plane. However, due to the effect of the mutual coupling proposed antenna can work only for the scan angle of $0° < \theta < 40°$ and $\varphi = 0°$ so that the side-lobe level is less than -10dB. Here the reduction of gain by approximately 3dB and increment in angular width is observed when compared to design without mutual coupling.

The design is then analyzed for the frequency downscaled design. The same analysis procedure is followed in this approach and approximately same results have been evaluated in the X-band design.

CHAPTER 4

TAPERED DIELECTRIC RESONATOR ROD ANTENNA

4.1 Introduction

Simple canonical structures provide efficient results, however according to one's need these structures can be modified to enhance the system performance such as impedance bandwidth, gain, radiation pattern and polarization. For next generation communication system the performance enhancement is a necessity. Therefore, the DRA is a best suited candidate for the setup as it supports a very distinguishing characteristic of design flexibility. One way to achieve this design flexibility is tapering. The edges of the canonical structure are cut to enhance the impedance bandwidth, thereby enhancing the system performance. Moreover it helps in achieving higher resonance frequency.

4.2 Related work

Various non-canonical structures have been studied till now. Almpanis et al [41], have designed an aperture fed dual bridge-dielectric resonator antenna (b-DRA) with high dielectric permittivity. This proposed antenna exhibits broadside multimode radiation. By increasing the number of radiating elements, more impedance bandwidth is obtained. However, with increase in the number of elements, the mutual coupling between them increases and applies a limitation. Ultra-wideband (UWB) monopole integrated with DRA has been reported to enhance the bandwidth and provide ultra-wideband for wireless communication. A hybrid monopole conical and hemispherical dielectric ring resonator (DRR) is presented [43]. The monopole of permittivity 10 is inserted at the center of both the DRRs. The proposed hemispherical monopole DRR obtains 25% large impedance bandwidth than the former cylindrical DRA version, however, the gain and radiation properties remain identical. The authors have observed that proposed antenna exhibits 126% impedance bandwidth and 4dBi gain.

Li et al [44] have attached a trapezoidal monopole patch on the DR concave surface as a feeding element. The antenna is oriented in a way that a metal plate is layered over the top of DR and air

gap is inserted in between DR and ground plane. The antenna obtains an impedance bandwidth of more than 75% from 2.9GHz to 6.7GHz with stable gain, consistent broadside radiation pattern and high radiation efficiency which can be used for wideband applications such as WiMAX and WLAN. However, this prototype is not profitable for terahertz communication due to presence of metal surface. Kumar and Gupta [56] have designed two different antenna geometries for the enhancement of bandwidth and gain. The first geometry is Gammadion cross DRA with semi-cylindrical slot (GCDRA-1) and second geometry is Gammadion cross DRA with rectangular slots (GCDRA-2) and both the designs are probe fed. It is observed that the bandwidth widens by the use of slots. The bandwidth of 31.6% and a peak gain of ~7 dBi at 5.1 GHz is obtained. These designs cover most of the wireless systems like C-band, 5.2, 5.5 and 5.8 GHz WLAN and WiMAX applications. The new proposed GCDRA-2 reduces the volume of DRA by 50% and enhances the bandwidth from 10 to 31.6% from reference antenna.

For circular polarization the basic design can be modified. Fang et. al. [75] have proposed a dual band circularly polarized DRA in which the corners of the DRA are removed at 45˚ and a diagonal groove\slit is inserted at the top of the DR. The antenna is fed by aperture coupled feeding exciting the quasi- TE_{111} and TE_{113} modes. 6.30% and 3.68% are the measured lower and upper band AR bandwidths, respectively. Moreover two unequal diagonal slits are loaded at the wall of the RDRA for wideband CP [76]. The proposed antenna is excited by the tapering strip which is connected by the microstrip line at one side and matched with a chip resistor at the other side. This antenna gives multimode radiation with 3 dB AR impedance bandwidth of 43-50% at 3.7 GHz, gain in between 4 and 6 dBi and radiation efficiency of more than 87%.

In this chapter, to up shift the resonance frequency and to enhance the impedance bandwidth of the simple DRRA structure, the tapering of the DRRA is done in a conical fashion using a detailed parametric analysis.

4.3 Parametric analysis of the Tapered DRRA

The tapering of the radiator is performed over the same proposed design. In this the DRR above the maximum touching height of the probe is down tapered, as shown in Figure 4.1. In this the tapering is done in conical fashion. The bottom radius of the cone is equal to *a*, whereas the top

radius a_t of the cone is varied to obtain an optimized structure. The dielectric permittivity of the DRR is chosen same. The design is then simulated.

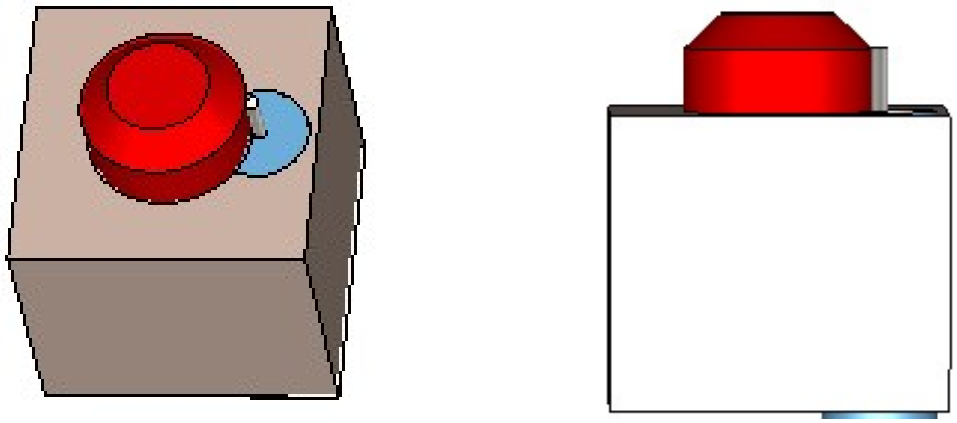

Figure 4.1: Down tapered DRRA (a) top view, (b) side view

4.4 Results

The DRR above 0.165mm is down tapered. It is observed that as the radius of the DRR decreases, i.e., more tapering occurs, the resonance frequency shifts upwards. This is observed with the help of parametric sweep, as shown in Figure 4.2. Then, by using the optimizer an optimized a_t is chosen.

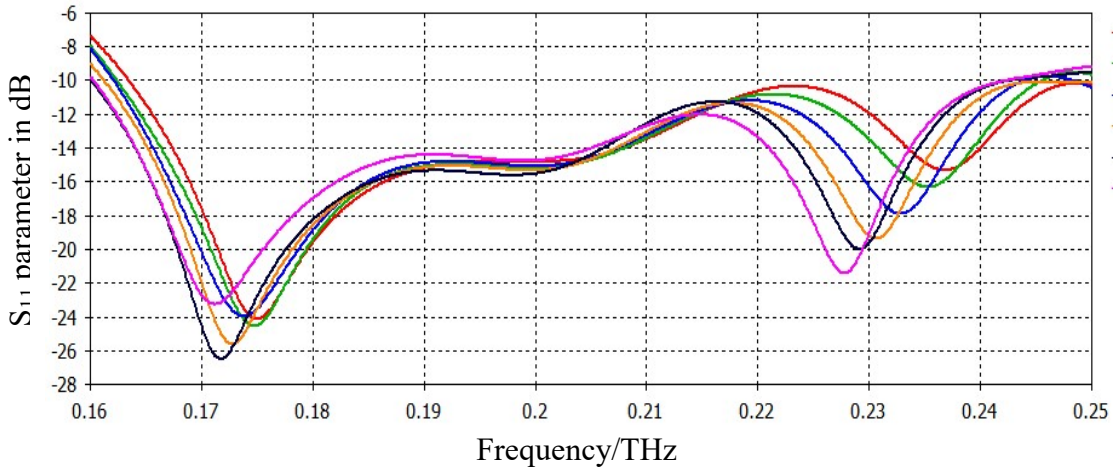

Figure 4.2: The parametric sweep applied to a_t.

Table 4.1: Resonance frequency for various

a_t (mm)	Resonance frequency (THz)	S-parameter (dB)	Bandwidth (GHz)
0.23 (pink)	0.171	-23.3	80.7 (160.13-240.9)
	0.227	-21.4	
0.19 (black)	0.172	-26.5	81.2 (160.13-241.4)
	0.229	-19.9	
0.15 (orange)	0.173	-25.5	81.9 (161.2-243.18)
	0.230	-19.3	
0.11 (blue)	0.1738	-23.9	82.06 (162-244.06)
	0.233	-17.9	
0.07 (green)	0.1746	-24.5	83.9 (162.6-246.59)
	0.235	-16.3	
0.03 (red)	0.175	-24.1	85 (163.5-248.2)
	0.237	-15.3	

From Table 4.1, it is observed that as the top radius of a_t decreases, the resonance frequency gets up shifted, whereas the impedance bandwidth of the design also increases. By using optimizer in CST, the best optimized S-parameter is obtained at a_t = 0.19mm. The design is then simulated and resonant at 0.172 and 0.229 THz. The impedance bandwidth of 81.9 GHz ranging from 0.160 THz to 0.242 THz is obtained, as shown in Figure 4.3.

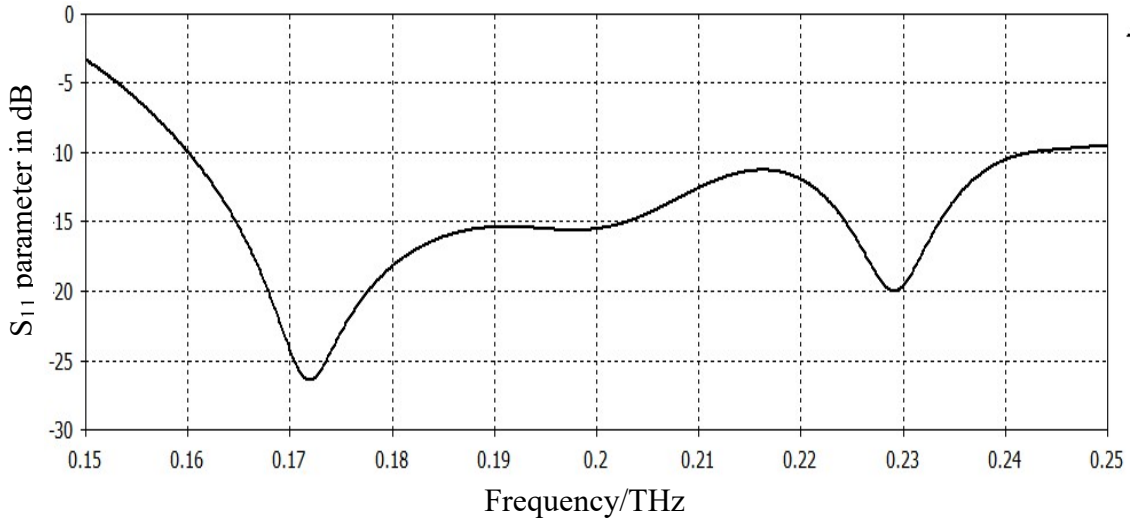

Figure 4.3: S-parameter for down tapering

The far field analysis is done for 0.172THz where the gain, directivity and efficiency of 8.188 dB, 8.22 dBi and 98%, respectively is obtained. It is observed that main lobe is directed towards 10˚, with 3-dB angular width of 65.9˚ in E-plane whereas in H-plane the magnitude of the main beam is 7.87 dB with main lobe at 0˚ and angular width of 66.9 dB, as shown in Figure 4.4.

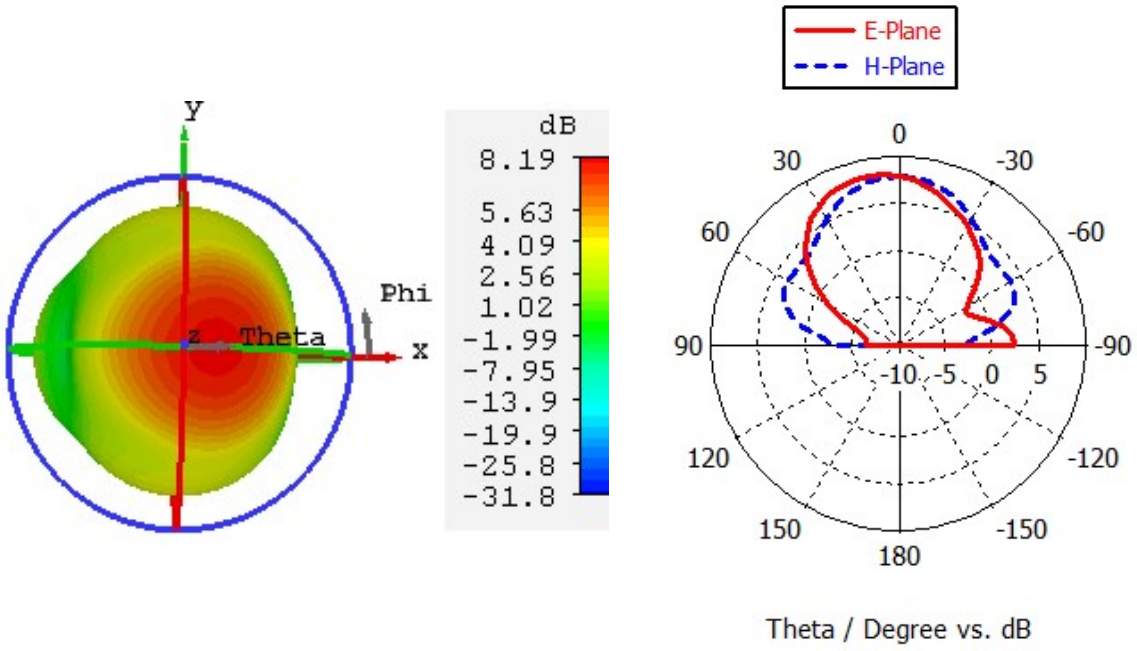

(a) (b)

Figure 4.4: The 3D far-field pattern (gain) and polar plot for E-plane and H-plane.

4.5 Conclusion

In this chapter, the variation of the tapering is observed at different values of a_t where a_t is the top cut radius of the cylinder. By parametric sweep it is observed that as the tapering radius is decreases, the frequency up shifts and the impedance bandwidth increases as well. The best optimized result of a_t =0.19mm is then extracted using the optimizer in CST. This design after simulation provides an impedance bandwidth of 81.9 GHz which is greater than that of the canonical structure, with two resonance frequency dips at 0.172 THz and 0.229 THz. At 0.272 THz the gain, directivity and efficiency of 8.188 dB, 8.22 dBi and 98%, respectively is obtained. Therefore, it is observed that this design helps in the enhancement of the bandwidth of the system.

CHAPTER 5

TAPERED DIELECTRIC RESONATOR ROD ANTENNA PHASED ARRAY

5.1 Introduction

With the enhancement of the bandwidth, the gain is also required to be enhanced for next generation communication. The design modification with the implementation of array provides better system performance and with the help of beam-steering a large area can be covered for communication purpose.

5.2 Related work

The modification of the designs as stated early enhances the design performance. Khalily et. al. [74] have investigated RDRA for both linear and circular polarization. Omnidirectional LP DRA is fed by coaxial probe and impedance bandwidth of 130 MHz from 5.15 to 5.35 GHz is obtained. However, by inserting several inclined slits to top wall, sidewalls and diagonals of a linearly polarized RDRA, degenerating modes are excited and generates circular polarization. This structure provides the 210 MHz AR bandwidth around 5.2 GHz. on the other hand, Mukharjee et al [60] have proposed a half hemispherical DRA with an array of slots (ϵ_r = 9.2). Periodic holes are drilled to increase the impedance bandwidth and lower down the Q factor. The measured 10 dB bandwidth is about 1 GHz (17.74%). Authors have varied the probe length and at 2.5cm, a bandwidth of 1.3 GHz (29%) and gain of 7.2dBi have been obtained for 4.5 GHz resonant frequency. The authors have suggested using this antenna for wideband applications.

Haraz et al [63] have proposed an array using four circular-shaped DD patch radiator fed by Wilkinson power divider (WPD). The proposed antenna is designed for 28GHz short range 5G wireless communication systems. A dielectric is used as a superstrate to increase the gain. To improve radiation, a uniplanar electromagnetic bandgap unit cell ground structure is used. The measured impedance bandwidth of proposed array antenna ranges from 27 to beyond 37 GHz and total realized gain is more than 16dBi. The authors have studied that this proposed design has

better radiation and efficiency characteristics than conventional metallic patch array. However, Li and Luk [64] have proposed a perforated DD patch antenna for an array, fed by a single layered substrate integrated waveguide (SIW) network. The 4x4 prototype has an impedance bandwidth of 23%, the gain up to 17.5dBi with cross polarization levels of less than -20dB are achieved at 60GHz. Because of good performance the authors suggests this proposed antenna array is good for millimeter wave applications.

In this Chapter, the phased array of the tapered DRA is analyzed using the Taylor current distribution. The beam-steering is also performed.

5.3 Parametric analysis

Sixteen individually tapered DRA elements are combined together as shown in Figure 5.1, to form a planar phased array configuration. The dimension of each element is same and every element is phase shifted independently. The spacing between individual DRRA elements (center to center) is *d*. To reduce the sidelobe level, the spacing between the element is taken $d=\lambda/2$, where λ is the resonant wavelength of the proposed antenna.

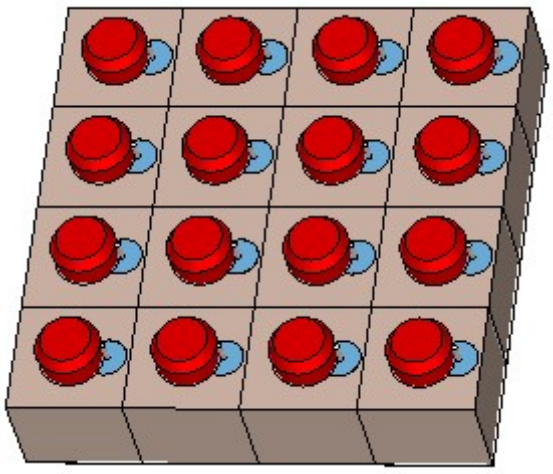

Figure 5.1: Array configuration for tapered DRRA

5.4 Results

The tapered antenna is analyzed for the Taylor current distribution. This non-uniform distribution helps in the reduction of the sidelobe levels. The design is then simulated for different scan angles. It is observed that for the scan angle of $0° < \theta < 40°$ and $\varphi = 0°$, the relative sidelobe level remains lower than -10dB.

The antenna is first scan in single direction, i.e., the progressive phase shift is applied in x-direction only while keeping the variation in y-direction constant (equal to 0). The results are shown in Figure 5.2 and Table 5.1 and 5.2.

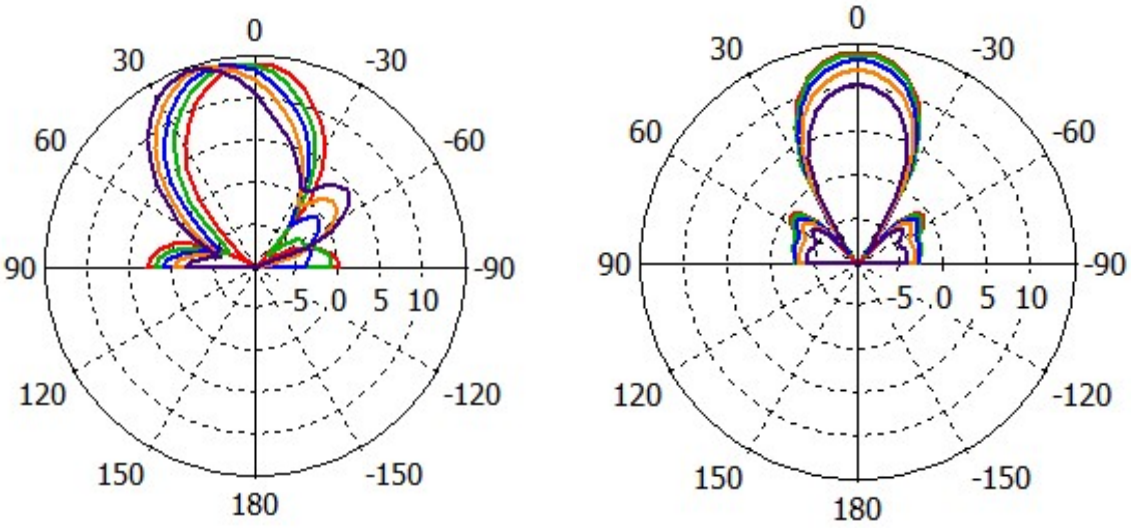

(a) (b)

Figure 5.2: Beam-steering at angle 0˚(red), 10˚(green), 20˚(blue), 30˚(pink) and 40˚(purple) at (a) E-Plane and (b) H-Plane

Table 5.1: For E-plane progressive phase shift in x-direction for Taylor distribution.

Progressive Phase shift (deg)	Main lobe magnitude (dB)	Main lobe direction (deg)	Angular width (dB)	Sidelobe level (dB)
0	14.2	0	35.6	-11.5
10	14.2	5	36	-12.4
20	14.2	10	36	-13.3
30	14.3	15	34.6	-13.2
40	14.5	20	32.4	-10.4

Table 5.2: For H-plane progressive phase shift in x-direction for Taylor distribution.

Progressive Phase shift (deg)	Main lobe magnitude (dB)	Main lobe direction (deg)	Angular width (dB)	Sidelobe level (dB)
0	14.2	0	33.6	-14.8
10	13.9	0	33.5	-14.9
20	13.2	0	33.4	-14.8
30	12.1	0	33.2	-14.6
40	10.4	0	33.2	-14.2

It is observed that with every 10˚ sweep of the scan angle, the main beam shifts by 5˚ in E-plane with approximately same magnitude whereas in the H-plane the magnitude decreases with each sweep. Moreover, it is observed that the 3 dB angular width of this proposed antenna is narrower than the canonical antenna presented in chapter 3 due to the high resonance frequency.

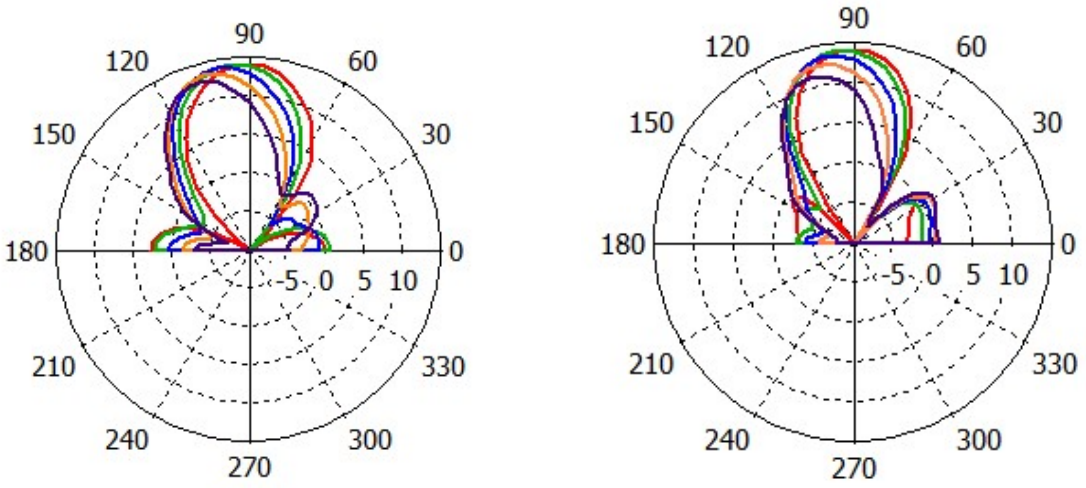

(a) (b)

Figure 5.3: Beam-steering at angle 0˚(red), 10˚(green), 20˚(blue), 30˚(orange) and 40˚(purple) at (a) E-Plane and (b) H-Plane

The antenna is then scanned in both xy-direction and the results are shown in Figure 5.3 and Table 5.3 and 5.4.

Table 5.3: For E-plane progressive phase shift in xy-plane for Taylor distribution.

Progressive Phase shift (deg)	Main lobe magnitude (dB)	Main lobe direction (deg)	Angular width (dB)	Sidelobe level (dB)
0	14.2	0	35.6	-11.5
10	14.2	5	34.6	-12.0
20	13.9	10	33.9	-13.4
30	13.4	15	32.7	-14.1
40	12.6	20	31	-11.8

Table 5.4: For H-plane progressive phase shift in xy-plane for Taylor distribution.

Progressive Phase shift (deg)	Main lobe magnitude (dB)	Main lobe direction (deg)	Angular width (dB)	Sidelobe level (dB)
0	14.2	0	33.6	-14.8
10	14	5	33.8	-14.8
20	13.4	5	33.1	-13
30	12.5	10	31.6	-11.4
40	11.3	15	30.4	-9.8

From the results, it is observed that with every 10˚ shift in the scanning angle, the main beam gets shifted approximately 5˚ in E-plane and H-plane. However, with each sweep the magnitude of the main lobe decreases.

5.5 CONCLUSION

In this chapter, the down tapered DRA is analyzed. Firstly, the frequency scanning is performed in x-direction for $0° \le \theta \le 40°$ while keeping θ constant in y-direction. The beam variation is only observed in E-plane of 5˚ for each 10˚ scan angle. Further, the frequency scanning is done in both the direction of orientation of the elements for $0° \le \theta \le 40°$ and observed that for every 10˚ phase shift, the main beam gets shifted in both the plane with reduction in magnitude with every sweep. It is also observed that the reduced 3 dB angular width is produced by the tapered DRA than that of canonical DRA.

CHAPTER 6

CONCLUSION AND FUTURE WORK

The terahertz regime of the electromagnetic spectrum is the most suitable entrant for the next generation communications system which demands huge bandwidth with high operating frequency for high data-rate communication. The terahertz communication link is advantageous over the microwave- and infrared-link due to its wide bandwidth and less atmospheric losses, respectively. However, there are various design issue arises in this unexplored regime of the spectrum with the increase in operating frequency. Further, the high power sources are required to be developed with highly reliable detectors within the atmospheric attenuation window as the power radiated by the THz source is very less. The potential issues related to the attenuation of the wave due to water molecule, rain, fog, etc also poses a major challenge in long distance THz communication, therefore till now the THz link has been established for indoor or femtocell communication. Lastly, high gain antennas are required to meet the need for future communication. The high gain antennas play an important role in the implementation of THz communication link. This parameter enhances the link's overall length. The commercially used microstrip antenna is considered a suitable candidate for this link, however at high frequencies the conductor losses are greater and the obtained bandwidth is narrower. The high efficiency with wider bandwidth and low dielectric losses are major features of the dielectric resonator antenna making it more suitable than that of the microstrip antenna at THz frequency range. However, with huge bandwidth a trade off with gain and directivity occurs. Various techniques such as the use of metamaterial, frequency selective surface, photonic band gap material, etc have been reported as a very effective way of improving gain and directivity of the DRA.

In Chapter 2, a simple DRRA design is presented which resonant at two frequencies, i.e., 0.17THz and 0.229THz, with impedance bandwidth of 79.7GHz. At 0.17THz, gain, directivity and efficiency of 8.885 dB, 8.937 dBi and 98%, respectively is obtained. To estimate the results, the design is frequency down-scaled by a factor of 15. It is observed that both the antennas produce approximately same results where gain of 7.97 dB with directivity of 8.033 and efficiency of 98.5%, respectively is obtained. Now to enhance the gain, 4×4 DRRA phased array configuration is designed. The results are obtained with and without mutual coupling using

uniform and Taylor current distribution, respectively in Chapter 3. The results have shown that with mutual coupling, the system performance degrades by reduction in the gain by approximately 3dB and increment in the angular width. The same design is then evaluated for the frequency downscaled antenna and approximately same results are observed as that of the canonical DRRA.

In Chapter 4, the bandwidth is enhanced by modifying the DRRA design. In this, the tapering of the radiating structure is performed over the antenna edges. The significant optimization over radiator is performed. It is observed that at a_t=0.19mm, the antenna radiates at 0.172 THz and 0.229 THz, with a impedance bandwidth of 81.2 GHz. At 0.172 THz, gain, directivity and efficiency of 8.188 dB, 8.22 dBi and 98%, respectively is obtained. The simulated results have shown a significant shift in the resonance frequency with increased bandwidth. This structure is then analyzed for a 4×4 array structure using Taylor current distribution to enhance the gain in Chapter 5. It is observed that by doing so the angular width of this antenna array is obtained less in comparison to the canonical DRRA, which is good is the perspective of resolution.

However, for next generation communication, a dynamic system approach is required such that switching between present generation and next generation is feasible. The electronically reconfigurable DRA is capable to uphold the communication better than the mechanically reconfigurable DRA, as for next generation THz communication system, the software operated systems are more reliable and less cost effective. Hence the solid state DRA is better suited than liquid state DRA.

The system complexity will increase further when parameters, beam-steering and reconfiguration will be put together in the system, which is one of the major challenges for future work.

REFERENCES

[1] T. Kleine-Ostmann and T. Nagatsuma, "A Review on Terahertz Communications Research," J. Infrared, Millimeter, and Terahertz Waves, vol. 32, no. 2, pp. 143–71, Feb. 2011

[2] K. R. Jha and G. Singh, "Terahertz planar antennas for future wireless communication: A technical review", Infrared Physics & Technology, vol. 60, pp. 71-80, Sept 2013.

[3] I. F. Akyildiz, S. Nie, S. C. Lin, M. Chandrasekaran, "5G Roadmap: 10 Key enabling technologies", Computer Networks, vol. 106, pp. 17–48, Sept 2016.

[4] J. Federici and L. Moeller, "Review of terahertz and subterahertz wireless communications", J. Appl. Phys.107, pp. 111101/1-22, 2010.

[5] Y. Niu, Y Li, D. Jin, Li Su and A. V. Vasilakos, "A survey of millimeter wave communications (mmWave) for 5G: Opportunities and challenges", Wireless Networks, vol. 21, no. 8, pp. 2657–2676, November 2015.

[6] V. M. Patel, J. N. Mait, D. W. Prather, and A. S. Hedden, "Computational millimeter wave imaging: Problems, progress, and prospects", IEEE Signal Processing Magazine, vol. 33, no. 5, pp. 109-118, Sept 2016.

[7] H. S. Ghadikolaei, C. Fischione, G. Fodor, P. Popovski, M. Zorzi, "Millimeter wave cellular networks: A MAC layer perspective", IEEE Transactions on Communications, vol. 63, no. 10, pp. 3437-3458, Oct 2015.

[8] S. Rangan, T. S. Rappaport and E. Erkip, "Millimeter-wave cellular wireless networks: Potentials and challenges", Proceeding of IEEE, vol. 102, no. 3, pp. 366-385, March 2014.

[9] Q. Lai, G. Almpanis, C. Fumeaux, H. Benedickter, and R. Vahldieck, "Comparison of the radiation efficiency for the dielectric resonator antenna and microstrip antenna at Ka band", IEEE Transactions on Antennas and Propagation, vol. 56, no. 11, pp. 3589-3592, Nov 2008.

[10] David M. Pozar, "Microwave and RF Wireless Systems", New York, John Wiley & Sons, 2001.

[11] S. A Long, M. W. McAllister, and L. C. Shen, "The resonant cylindrical dielectric cavity antenna", IEEE Trans. Antennas Propag., vol. 31, no. 5, pp. 406-412, May 1983.

[12] M. W. McAllister, S. A. Long, and G. L. Conway, "Rectangular dielectric resonator antenna**",** Electronics Letters, vol. 19, no. 6, pp. 218-219, 1983.

[13] M. W. McAllister and S. A. Long, "Resonant hemispherical dielectric antenna", Electronics Letters, vol. 20, pp. 657-659, Aug 1984.

[14] A. Petosa and A. Ittipiboon, "Dielectric resonator antennas: A historical review and the current state of the art", IEEE Antennas and Propagation Magazine, vol. 52, no. 5, pp. 91-116, Oct 2010.

[15] J. Kumar and N. Gupta, "Performance analysis of dielectric resonator antenna", Wireless Pers Commun, vol. 75, pp. 1029-1049, Sept. 2013.

[16] K. M. Luk and K. W. Leung, "Dielectric Resonator Antennas" Hertfordshire, England: Research Studies Press, 2002.

[17] A. Ittipiboon, R. K. Mongia, Y. M. M. Antar, P. Bhartia and M. Cuhaci, "Aperture-fed rectangular and triangular dielectric resonators for use as magnetic dipole antennas," Electronic. Letters, vol. 29, pp. 2001-2002, Nov.1993.

[18] R. K. Mongia, A. Ittipiboon, P. Bhartia and M. Cuhaci, "Electric-monopole antenna using a dielectric ring resonator," Electronic Letters, vol. 29, pp. 1530-1531, Aug. 1993.

[19] K. W. Leung, K. Y. Chow, K. M. Luk and E. K. N. Yung, "Excitation of dielectric resonator antenna using a soldered-through probe," Electronic Letters, vol. 33, pp. 349 - 350, Feb. 1997.

[20] K. W. Leung, K. M. Luk and E. K. N Yung, "Spherical cap dielectric resonator antenna using aperture coupling", Electronic Letters., vol. 30, no. 17, pp. 1366-1367, Aug. 1994.

[21] G. P Junker, A. A Kishk, A. W Glisson, D. Kajfez, "Effect of air gap around the coaxial probe exciting a cylindrical dielectric resonator antenna", IEE Electron Letters, vol. 30, no. 3, pp. 177-178, Feb 1994

[22] G. P. Junker, A. A Kishk, and A. W. Glisson, "Input impedance of dielectric resonator antennas excited by a coaxial probe", IEEE Trans. Antennas and Propagation, vol. 42, no. 7, pp. 960-966, July 1994.

[23] G. Zhou, A. A. Kishk, and A. W. Glisson, "Input impedance of a hemispherical dielectric resonator antenna excited by a coaxial probe", Proc. EEE Antennas and propagation symposium, Ann Arbour, Michigan, June 1993, pp-1038-1041

[24] R. A. Kranenburg and S. A. Long, "Microstrip transmission line excitation of dielectric resonator antennas", Electronics Letters, vol. 24, no. 18, pp. 1156-1157, 1988.

[25] L. Kumar and N. Gupta, "A comparative study of different feeding mechanisms for rectangular dielectric resonator antenna", IUP Journal of Telecommunications, vol. 7, no. 1, pp. 39-47, Feb 2015.

[26] A. Ittipiboon, R. K. Mongia, Y. M. M. Antar, P. Bhartia, and M. Cuhaci, " Aperture fed rectangular and triangular dielectric resonators for use as magnetic dipole", IEE Electronics letters, vol. 29, no. 3, pp-2001-2002,1993.

[27] K. W. Leung, K. Y. A Lai, K. M. Luk, and D. Lin, "Input impedance of aperture coupled hemispherical dielectric resonator antenna", IEE Electronics Letters, vol. 29, pp. 1165-1167, 1993.

[28] A. A. Kishk, A. Ittipiboon, Y. M. M Antar and M. Cuhaci, "Dielectric resonator antenna fed by a slot in the ground plane of a microstrip line", Proc. 8th Int. Conf. on Antennas and Propagation, ICAP, part 1, April 1993, pp. 540-543

[29] R. Kranenberg, S. A Long, and J. T. Williams, "Coplanar waveguide excitation of dielectric resonator antennas", IEEE Transactions on Antennas and Propagation, vol. 39, pp. 119-122, Jan.1991.

[30] C Curry, "Novel size- reduced circularly polarized antennas", Master Thesis, Royal Military College, Kingston, Canada, July 2000.

[31] M. S Al Salameh, Y. M. M. Antar, G. Seguin, A. Petosa, “Analysis and measurement of compact-size DRA with CPW feed”, USNC/URSI National Radio Science Meeting, Boston, MA, July 2001, p. 221.
[32] J. P. S. McKenzie, “Dielectric resonator antennas fed by coplanar waveguide at extremely high frequency”, Master Thesis, Royal Military College, Kingston.
[33] M. T. Birand and R. V. Gelsthorpe, “ Experimental millimetric array using dielectric radiators fed by means of dielectric waveguide” IEE Electron Letters, vol. 17, no. 18, pp.633-635, Sept. 1981.
[34] D. Guha and C. Kumar, “Microstrip patch versus dielectric resonator antenna bearing all commonly used feeds”, IEEE Transactions on Antennas and Propagation Magazine, vol. 58, no. 1, pp. 45-55, Feb 2016.
[35] C.A. Balanis, “Modern Antenna Handbook”, John Wiley & Sons, 2008.
[36] R. C. Johnson, “Antenna Engineering Handbook”, McGraw-Hill, 1993.
[37] D. Guha, B. Gupta and Yahia M. M. Antar, “Hybrid monopole-DRAs using hemispherical/conical shaped dielectric ring resonators: Improved ultra-wideband designs”, IEEE Transactions of Antennas and Propagation, vol. 60, no. 1, pp. 393-398, Jan 2012.
[38] A. Sharma and S. C. Shrivastava, “Bandwidth enhancement techniques Of dielectric resonator antenna”, International Journal of Engineering Science and Technology, vol. 3, no. 7, pp. 5995-5999, July 2011.
[39] Y. Zhang, Z.N. Chen, X. Qing, and W. Hong, “Wideband millimeter-wave substrate integrated waveguide slotted narrow-wall fed cavity antennas”, IEEE Transactions on Antennas and Propagation, vol. 59, no. 5, pp. 1488-1496, May 2011.
[40] Meng Zou and Jin Pan, "Investigation of resonant modes in wideband hybrid omnidirectional rectangular dielectric resonator antenna", IEEE Transactions on Antennas and Propagation, vol. 63, pp. 3272-3275, 2015.
[41] Q. Lai, G. Almpanis, C. Fumeaux, W. Hong, and R. Vahldieck, “60 GHz aperture-coupled dielectric resonator antenna fed by a half mode substrate integrated waveguide”, IEEE Transactions on Antennas and Propagation, vol. 58, no. 6, pp. 1856-1864, June 2010.
[42] Y. Li and K. M. luk, “Wideband perforated dense dielectric patch antenna array for millimeter wave application”, IEEE Transactions on Antennas and Propagation, vol. 63, no. 8, pp. 3780-3786, August 2015.
[43] R. K. Gangwar, S. P. Singh, D. Kumar, “4-Element wideband rectangular dielectric resonator antenna terminated in a bio-medium”, Wireless Pers Commun, vol. 73, pp. 663-677, 2013.
[44] E. H. Lim and K. W. Leung, “Transparent Dielectric Resonator Antennas For Optical Applications,” IEEE Trans. Antennas Propag., vol. 58, no.4, pp. 1054–1059, Apr. 2010.

[45] C. Prachi, R. K. Chaudhary, and K. V. Srivastava, "Rounded bevel shaped fed cylindrical dielectric resonator antenna for wideband applications", Microwave and Optical Technology Letters, vol. 57, pp. 2364, 2015.

[46] Rajkishor Kumar and R. K. Chaudhary, "A wideband circularly polarized dielectric resonator antenna excited with conformal-strip and inverted L-shaped microstrip-feed-line for WLAN/WI-MAX applications", Microwave and Optical Technology Letters, vol. 58, pp. 2525, 2016.

[47] Muhammad Kamran Saleem, Majeed A. S. Alkanhal, and Abdel Fattah Sheta, "Switch beam dielectric resonator antenna array with four reconfigurable radiation patterns", Microwave and Optical Technology Letters, vol. 58, pp. 86, 2016.

[48] R.K. Chaudhary, H.B. Baskey, K.V. Srivastava, and A. Biswas, "Synthesis and microwave characterization of (Zr0.8Sn0.2)TiO4–epoxy composite and its application in wideband stacked rectangular dielectric resonator antenna", IET Microwaves Antennas & Propagation, vol. 6, pp. 740, 2012.

[49] R. K. Chaudhary, K. V. Srivastava, and Animesh Biswas, "Wideband multilayer multi-permittivity half-split cylindrical dielectric resonator antenna", Microwave and Optical Technology Letters, vol. 54, pp. 2587, 2012.

[50] Sajid Aqeel, Jamal Nasir, Aftab Ahmad Khan, Jalil ur Rehman Kazim, Mohd Haizal Jamaluddin, and Owais Owais, "Dual-band MIMO dielectric resonator antenna for WiMAX/WLAN applications", IET Microwaves Antennas & Propagation, vol. 11, no. 1, pp. 113-120, 2017.

[51] Nan Yang, Kwok Wa Leung, Eng Hock Lim, "Mirror-integrated dielectric resonator antenna", IEEE Transactions on Antennas and Propagation, vol. 62, pp. 27-32, 2014.

[52] Kwok W. Leung, Yong M. Pan, Xiao S. Fang, Eng H. Lim, Kwai-Man Luk, Hau P. Chan, "Dual-function radiating glass for antennas and light covers—Part I: Omnidirectional glass dielectric resonator antennas", IEEE Transactions on Antennas and Propagation, vol. 61, pp. 578-586, 2013.

[53] J. Kumar and N. Gupta, “Bandwidth and gain enhancement technique for Gammadion cross dielectric resonator antenna”, Wireless Pers Commun, vol. 85, pp. 2309-2317, 2015.

[54] R. Cicchetti, A. Faraone, E. Miozzi, R. Ravanelli, and O. Testa, “A high-gain mushroom-shaped dielectric antenna for wideband wireless applications”, IEEE Antennas and Wireless Propagation Letters, vol. 64, pp. 2848-2861, July 2016.

[55] N. Nasimuddin, Z.N. Chen, and X. ching, “Bandwidth enhancement of single-feed circularly polarized antenna using a metasurfaces”, IEEE Antennas and Propagation Magazine, vol. 58, no. 2, pp. 39- 46, April 2016.

[56] A. Kianinejad, T. N. Chen, L. Zang, W. Liu, and C.W. Qiu, “Spoof plasmon-based slow wave excitation of DRA”, IEEE Transactions of Antennas and Propagation, vol. 64, no. 6, pp. 2094-2099, June 2016.

[57] Biswajeet Mukherjee, Pragati Patel, Gopi Shrikanth Reddy, and J Mukherjee, "A novel half hemispherical dielectric resonator antenna with array of slots for wideband applications", Progress Electromagnetics Research C, vol. 36, pp. 207, 2013.

[58] Chengjun Zou, Philipp Gutruf, Withawat Withayachumnankul, Longfang Zou, Madhu Bhaskaran, Sharath Sriram, and C. Fumeaux, "Nanoscale TiO_2 dielectric resonator absorbers", Optics Letters, vol. 41, pp. 3391, 2016.

[59] B. Mukherjee, P. Patel, G. S. Reddy, and J. Mukherjee, "A novel half hemispherical dielectric resonator antenna with array of slots for wideband applications", Progress Electromagnetics Research, vol. 36, pp. 207-221, 2013.

[60] Y.F. Wang, S. Liu, T. A. Denidni, Q. S. Zeng, and G.Wei, "Integrated ultra wide band plannar monopole with cylindrical dielectric resonator antennas", Progress Electromagnetics Research, vol. 44, pp. 44-53, 2013.

[61] B. Sahu, P. Tripathi and S. P. Singh, "Investigation on cylindrical dielectric resonator antenna with metamaterial superstrate", Wireless Pers Commun, vol. 84, pp. 1151-1163, May 2015.

[62] K. W. Leung, X. S. Fang, Y. M. Pan, E. H. Lim, K. M. Luk, H. P. Chan, "Dual-function radiating glass for antennas and light covers—Part II: Dual-band glass dielectric resonator antennas", IEEE Transactions on Antennas and Propagation, vol. 61, pp. 587-597, 2013.

[63] X. S. Fang, K. W. Leung, "Linear-/circular-polarization designs of dual-/wide-band cylindrical dielectric resonator antennas", IEEE Transactions on Antennas and Propagation, vol. 60, no. 6, pp. 2662-2671, June 2012.

[64] Ru-Ying Sun, "Bandwidth enhancement of circularly polarized dielectric resonator antenna", ETRI Journal, vol. 37, no. 1, pp. 26-31, Feb 2015.

[65] O. M. Haraz, A. Elboushi, S. A. Alshebeili, and A. R. Sebak, "Dense dielectric patch array antenna with improved radiation characteristics using EBG ground structure and dielectric superstrate for future 5G cellular network", IEEE Access, vol. 2, pp. 909-913, Sept 2014.

[66] R. K. Mongia, A. Ittipiboon, and M. Cuhaci, "Measurement of radiation efficiency of dielectric resonator antennas", IEEE Microwave and Guided wave Letters, vol. 4, no. 3, pp. 80-82, 1991

[67] R. Deng, F. Yang, S. Xu, and P. Pirinoli, "Terahertz reflectarray antennas: An overview of the state-of-the-art technology", International Conference on Electromagnetics in Advanced Applications (ICEAA), Aruba, 3-8 Aug, 2014, pp. 667-670.

[68] Ahmed Z. Ashoor, and Omar M. Ramahi, "Dielectric resonator antenna arrays for microwave energy harvesting and far-field wireless power transfer", Progress Electromagnetics Research C, vol. 59, pp. 89, 2015.

[69] M. Decker , I. Staude, M. Falkner, J. Dominguez, D. N. Neshev, I. Brener, T. Pertsch, Y. S. Kivshar, "High-Efficiency Dielectric Huygens' Surfaces", Adv. Optical Mater., vol. 3, pp. 813–820, 2015.

[70] Idris Messaoudene, Tayeb A. Denidni, and Abdelmadjid Benghalia, "CDR antenna with dual-band 1.9/2.7 GHz for MIMO-LTE terminals", Microwave and Optical Technology Letters, vol. 57, no. 10, pp. 2388-2391, 2015.

[71] R. Kumar and R. K. Chaudhary, "A wideband circularly polarized cubic dielectric resonator antenna excited with modified micorstrip feed", IEEE Antennas and Wireless Propagation Letters, vol. 15, pp. 1285-1288, 2016.

[72] B. Rana and S. K. Parui, "High gain circularly-polarized dielectric resonator antenna array with helical exciter", Progress Electromagnetics Research Letters, vol. 44, pp. 107-111, 2014.

[73] R. Kumari and R. K. Gangwar, "Circularly polarized dielectric resonator antennas: Design and development", Wireless Pers Commun, vol. 86, pp. 851-886, July 2015.

[74] Xiaosheng Fang, Kwok Wa Leung, and Eng Hock Lim, "Singly-Fed Dual-Band Circularly Polarized Dielectric Resonator Antenna", IEEE Antennas and Wireless Propagation Letters, vol. 13, pp. 995-998, 2014.

[75] Mohsen Khalily, M R. Kamarudin, and Mohd H. Jamaluddin, "A novel square dielectric resonator antenna with two unequal inclined slits for wideband circular polarization", IEEE Antennas and Wireless Propagation Letters, vol. 12, pp. 1256-1259, 2013.

[76] Jing Liu, Shun-Shi Zhong, and R.-C. Han, "Broadband circularly polarised dielectric resonator antenna fed by wideband switched line coupler", Electronics Letters, vol. 50, pp. 725, 2014.

[77] S. Fakhte, H.Oraizi, R. Karimain and R. Fakhte, "A new wideband circularly polarized staired-shaped dielectric resonator antenna", IEEE Transactions on Antennas and Propagation, vol. 63, no. 4, pp. 1828-1832, April 2015.

[78] Rong-Cang Han, Shun-Shi Zhong, and Jing Liu, "Design of broadband circularly polarized dielectric resonator antenna using improved feed network", Microwave and Optical Technology Letters, vol. 56, pp. 2191, 2014.

[79] Rajkishor Kumar and R K Chaudhary, "Modified microstrip-line-fed rectangular dielectric resonator antenna coupled with slotted ground plane for wideband circular polarization", Microwave and Optical Technology Letters, vol. 58, pp. 206, 2016.

[80] Mohsen Khalily, Muhammad R. Kamarudin, Mastaneh Mokayef, and Mohd H. Jamaluddin, "Omni-directional circularly polarized dielectric resonator antenna for 5.2-GHz WLAN applications", IEEE Antennas and Wireless Propagation Letters, vol. 13, pp. 443-446, 2014.

[81] S. Fakhte, H.Oraizi and R. Karimain, "A novel low-cost circularly polarized rotated stacked dielectric resonator antenna", IEEE Antennas and Wireless Propagation Letters, vol. 13, pp. 722-725, 2014.

[82] M. Zhang, B. Li, and X. Lv, "Cross-slot-coupled wide dual-band circularly polarized rectangular dielectric resonator antenna", IEEE Antennas and Wireless Propagation Letters, vol. 13, pp. 532-535, 2014.

[83] Min Guo, Xiao-Bo Xuan, Min Wang, Jun Wen Cui, and Shun-Shi Zhong, "A high-isolation dual-polarization dielectric resonator antenna with bowtie-shaped slot coupling", Microwave and Optical Technology Letters, vol. 57, pp. 2426, 2015.

[84] Ubaid Ullah, Wan Fahmin Faiz Wan Ali, Mohd Fadzil Ain, Nor Muzlifah Mahyuddin, and Zainal Arifin Ahmad, "Design of a novel dielectric resonator antenna using MgTiO3–CoTiO3 for wideband applications", Materials & Design, vol. 85, pp. 396, 2015.

[85] L. Zou, D. Abbott, and C. Fumeaux, "Omni-directional Cylindrical dielectric resonator antenna with dual polarization", IEEE Antennas and Wireless Propagation Letters, vol. 11, pp. 515-518, 2012

[86] Rajkishor Kumar and R K Chaudhary, "A new modified CPW-fed wideband circularly polarized half-split cylindrical dielectric resonator antenna with different permittivity of two layers in radial direction", International Journal of RF and Microwave Computer-Aided Engineering, vol. 27, no. 3, pp. 1-9, 2016.

[87] Prachi Chauthaiwale, R K Chaudhary, and K V Srivastava, "Circularly polarized bowtie-shaped dielectric resonator antenna excited with asymmetric cross slot", Microwave and Optical Technology Letters, vol. 57, pp. 1723, 2015.

[88] Meng Zou and Jin Pan, "A simple dual-band circularly polarized rectangular dielectric resonator antenna", Progress Electromagnetics Research Letters, vol. 53, pp. 57, 2015.

[89] M. T. Aligodarz, D. M. Klumyshyn, A. Rashidin, M. Börner, L. Shafai, and J. Mohr, "Investigation on photoresist-based artificial dielectrics with tall embedded metal grids and their resonator antenna application", IEEE Transactions on Antennas and Propagation, vol. 63, no. 8, pp. 3826-3838, Sept 2015.

[90] Ru-Ying Sun and Qing-Hu Chen, "Quadrature feed wideband circularly polarized cylindrical dielectric resonator antenna", Journal of Electromagnetic Waves and Applications, vol. 28, pp. 10-11, 2014.

[91] R. L. Haupt and M. Lanagan, "Reconfigurable antennas", IEEE Antennas and Propagation Mazagine, vol. 55, no. 1, pp. 49-61, Feb 2013.

[92] H. L. Zhu, X. H. Liu, S. W. Cheung, and T. I. Yuk, "Frequency reconfigurable antenna using metasurface," IEEE Trans. Antennas Propag., vol. 62, no. 1, pp. 80–85, Jan. 2014.

[93] L. Ge and K. M. Luk, "Band-reconfigurable unidirectional antenna", IEEE Antennas and Propagation Magazine, vol. 52, no. 5, pp. 18-27, April 2016.

[94] R. Gupta and R. Yaduvanshi, "Reconfigurable aperture coupled rectangular dielectric resonator antenna", Proc. 2nd International Conference on Computing for Sustainable Global Development (INDIACom), India, 11-13 Mar, 2015, pp. 859-862.

[95] L. Zou and C. Fumeaux, "A cross-shaped dielectric resonator antenna for multifunction and polarization diversity applications", IEEE Antennas and Wireless Propagation Letters, vol. 10, pp. 742-745, 2011.

[96] H. K. Ng and K. W. Leung, "Frequency tuning of the linearly and circularly polarized dielectric resonator antennas using multiple parasitic strips," IEEE Trans. Antennas Propag., vol. 54, no. 1, pp. 225–230, Jan. 2004.

[97] S. V. Hum and J. Perruisseau-Carrier, “Reconfigurable reflectarrays and array lenses for dynamic antenna beam control: A review”, IEEE Ants. and wireless prop. letters, vol. 62, pp. 183-198, Jan 2014

[98] A. Petosa, “Frequency agile antennas for wireless communication- A survey”, Proc. 14th International Symposium on Antenna Technology and Applied Electromagnetics and American Electromagnetics Conference, 2010, pp. 1-4.

[99] J. McDonald and G. H. Huff, “Microfluidic mechanisms for reconfigurable dielectric resonator antennas,” URSI Gen. Assembly, Chicago, IL, 2008.

[100] G.H. Huff, D.L. Rolando, P. Walters, and J. McDonald, “A frequency reconfigurable dielectric resonator antenna using colloidal dispersion”, IEEE Antennas and Wireless Propagation Letters, vol. 9, pp. 288-290, 2010.

[101] G. O’Keefe and S. P. Kingsley, “Tunability of liquid dielectric resonator antennas,” IEEE Antennas Wireless Propagation Letters, vol. 6, pp. 533–536, 2007.

[102] M. Zou, J. Pan, and Z. Shen, “Frequency-reconfigurable water dielectric resonator antenna”, Proc. 17th International Symposium on Antenna Technology and Applied Electromagnetics (ANTEM), QC, Canada, 10-13 July 2016, pp-1-4.

[103] L. A. Shaik, C. Saha and S. Arora, “Bandwidth reconfigurable cylindrical dielectric ring resonator antenna with metallic loading”, Proc. IEEE Applied electromagnetics conference (AEMC), Guwahati, India, 18-21 Dec, 2015, pp. 1-2.

[104] J. Li, T. A. Denidni, and Q, Zeng, “High gain reconfigurable millimeter-wave dielectric resonator antenna”, Proc. IEEE International Symposium on Antennas and Propagation & USNC/URSI National Radio Science Meeting, Vancouver, BC, Canada, July 19 -24 2015, pp. 444-445.

[105] R. Ghosal and B. Gupta, “Design of reconfigurable band notched Ultra Wide Band(UWB) stacked DRA using metamaterial structure”, Proc. International Conference and Workshop on computing and communications (IEMON), Vancouver, BC, Canada, 15-17 Oct, 2015, pp. 1-4

[106] F. F. W. Ali, M. Othman, Mohd F. Ain, N. Shah Abdullah, and Z. A. Ahmad, “The behavior of high frequency tunable dielectric resonator antenna (DRA) with the addition of excess Fe_2O_3 in $Y_3Fe_5O_{12}$ (YIG) formulation”, J Mater Sci: Mater Electron, vol. 25, pp. 560–572, 2014.

[107] M. Abdallah, W. M. Abdel-Wahab, Ying Wang, and S. Safavi-Neini, “A tunable circuit model for the modeling of dielectric resonator antenna array”, IEEE Antennas and Wireless Propagation Letters, vol. 15, pp. 830-833, 2016

[108] Jie-Bang Yan and J. T. Bernhard, “Design of a MIMO dielectric resonator antenna for LTE femtocell base stations,” IEEE Trans. Antennas and Propagation, vol. 60, no. 2, pp. 438-444, Feb. 2012.

[109] Z. Li, C. Wu, and J. Litva, "Adjustable frequency dielectric resonator antenna," Electronics Letters, vol. 32, no.7, pp. 606-607, March 1996

[110] A. Petosa and S. Thirakoune, “Frequency tunable rectangular dielectric resonator antenna”, Proc. IEEE Antennas and Propagation Society International Symposium, North Charleston, SC, USA, June 1-5, 2009, pp. 1-4

[111] C.Y. Huang, "Slotted ground plane for frequency tunable dielectric resonator antenna," Microwave and Optical Technology Letters, vol. 35, no.3, pp. 193-195, Nov. 2002

[112] C. Y. Huang and C. W. Ling, “Frequency-adjustable circularly polarized dielectric resonator antenna with slotted ground plane,” Electronics Letters, vol. 39, pp. 1030–1031, Jul. 2003

[113] M. K. Saleem,M. A. S. Alkanhal, A. F. Sheta, “Dual strip-excited dielectric resonator antenna with parasitic strips for radiation pattern reconfigurability”, International Journal of Antennas and Propagation, vol. 2014, pp.1-7, 2014.

[114] K. K. So and K. W. Leung, “Bandwidth enhancement and frequency tuning of the dielectric resonator antenna using a parasitic slot in the ground plane,” IEEE Trans. Antennas Propag., vol. 53, no. 12, pp. 4169–4172, Dec. 2005.

[115] J. B. Yan and J.T. Bernhard, “Implementation of a frequency-Agile MIMO dielectric resonator antenna”, IEEE Transaction of Antenna and Prop., vol. 61, no. 7, pp. 3434-3441, 2013.

[116] H. K. Ng and K.W. Leung, “Frequency tuning of the dielectric resonator antenna using a loading cap,” IEEE Trans. Antennas Propag., vol. 53, no.3, pp. 1229–1232, Mar. 2005.

[117] H. K. Ng and K. W. Leung, “Frequency tuning of the linearly and circularly polarized dielectric resonator antennas using multiple parasitic strips,” IEEE Trans. Antennas Propag., vol. 54, no. 1, pp. 225–230, Jan. 2004.

[118] S. Nikolaou, K. Boyon, and P. Vryonides, "Reconfiguring antenna characteristics using PIN diodes," Proceedings 3rd European Conference on Antennas and Propagation, Berlin, 2009, pp. 3748-3752.

[119] J. Desjardins, D. A. McNamara, S. Thirakoune, and A. Petosa, “Electronically frequency-reconfigurable rectangular dielectric resonator antennas,” IEEE Trans. Antennas Propag., vol. 60, no. 6, pp. 2997–3002, Jun. 2012

[120] S. M. Salman, S. K. Khamas, and G. G. Cook, “Slot fed SPIN diode dielectric resonator antenna”, Proc. Ant. and Prop. Conf. (LAPC), Loughborough, UK, 10 – 11 Nov 2014, pp. 336-339.

[121] S. Danesh, S. K. A. Rahim, M. Abedian, M. R. Hamid, and M. Khalily, “Frequency-reconfigurable rectangular dielectric resonator antenna”, IEEE Antennas and Wireless Propagation Letters, vol. 12, pp. 1331-1333, 2013.

[122] S. Danesh, T. A. Rahman, M. Abedian, M. R. Kamarudin, and M. Khalily, “A wideband frequency reconfigurable rectangular dielectric resonator antenna”, Proc. 10th European Conference on Antennas and Propagation (EuCAP), Davos, Switzerland, 10-15 April, 2016, pp. 1-4.

[123] R. D. Gupta and M. S. Parikar, “Bandwidth reconfigurable dielectric resonator antenna”, Proc. Ant and Prop. conf. (LAPC), Loughborough, UK, 10 – 11 Nov, 2014, pp. 473-475.

[124] S. Danesh, S. K. A. Rahim, and M. Abedian, "Frequency reconfigurable rectangular dielectric resonator antenna for WiMAX/WLAN applications" Microwave and Optical Technology Letters, vol. 57, no. 3, pp. 579-582, 2015.

[125] S. Danesh, S. K. A. Rahim, M. Abedian, and M. R. Hamid, "A compact frequency-reconfigurable dielectric resonator antenna for LTE/WWAN and WLAN application", IEEE Antennas and Wireless Propagation Letters, vol. 14, pp. 486-489, 2015.

[126] R. Khan, J. ur R. Kazim, A. A. Khan, S. Aqeel, and Owais, "A reconfigurable dielectric resonator antenna with pattern diversity for DVB-H application", Proc. International Conference on Intelligent Systems Engineering (ICISE), Islamabad, Pakistan, 15-17 Jan, 2016, pp. 1-4.

[127] B. Dwivedi, S. K. Behera, "Frequency reconfigurable DRA array using wideband Wilkinson's approach", Proc. Global conference on communication technologies (GCCT), Thuckalay, Tamil Nadu, India, 23 April-24 April 2015, pp. 655-658.

[128] C. X. Hao, B. Li, K.W. Leung, and X. Q. Sheng, "Differentially fed dielectric resonator antenna loading with capacitive elements for frequency response reconfigurability", Proc. IEEE international conference on Microwave technology & computational electromagnetics (ICMTCE), Beijing, China, 22 May -25 May 2011, pp. 19-22.

[129] C. X. Hao, B. Li, K. W. Leung, and X. Q. Sheng, "Frequency-tunable differentially fed rectangular dielectric resonator antennas," IEEE Antennas Wireless Propagation Letters, vol. 10, pp. 884–887, 2011

[130] T. Apperley and M. Okoniewski, "An air gap-based frequency switching method for the dielectric resonator antenna", IEEE Antenna and Wireless Propagation Letters, vol. 13, pp. 455-458, 2014.

[131] G. N. Malheiros-Silveira, G. S. Wiederhecker, and H. E. Hernández-Figueroa, "Dielectric resonator antenna for applications in nanophotonics", *Optical Express,* vol. 21, No. 1, pp-1234-1237, Jan 2013

[132] L. Zou, W. Withayachumnankul, C. M. Shah, A. Mitchell, M. Bhaskaran, S. Sriram, and C. Fumeaux, "Dielectric resonator nano-antennas at visible frequencies", *Optical Express,* vol. 21, no. 1, pp.1344-1352, Jan 2013.

[133] L. Zou, W. Withayachumnankul, C. M. shah, A. Mitchell, M. Klemm, M. Bhaskaran, S.Sriram, and C. Fumeaux, "Efficiency and scalability of dielectric resonator antennas at optical frequencies", *IEEE Photonics Journal,* vol. 6, no. 4, pp. 4600110 /1-11, August 2014.

[134] M. K. Saleem, M. Abdel-Rahman, M. Alkanhal, A. Sebak, "A cylindrical dielectric resonator antenna-coupled sensor configuration for 94GHz detection", *International Journal of Antennas and Propagation,* vol. 2014, pp. 1-4, 2014.

[135] X. D. Deng, Y. Li, C. Liu, W. Wu, Y. Z. Xiong, "340 GHz on-chip 3-D antenna with 10 dBi gain and 80% radiation efficiency", *IEEE Transactions on Terahertz Science and Technology*, vol. 5, no. 4, pp. 619-627, July 2015.

[136] S.H. Choi, I.J. Lee, S. Jeon, and M. Kim, "A 280-GHz rectangular cavity aantenna integrated in 80-μm InP substrate", *IEEE Antennas and Wireless Propagation Letters*, pp. 1-3, DOI: 10.1109/LAWP.2016.2606650, 2016.

[137] Georgios Almpanis, "On the geometry and the coupling schemes of broadband dielectric resonator antennas", PhD Thesis, Swiss Federal Institute Of Technology Zurich, 2009.

[138] D. Headland, W. Withayachumnankul, S. Nirantar, M. Bhaskaran, S. Sriram, and C. Fumeaux, "High efficiency dielectric resonator antennas in the terahertz range", *Proc. IEEE MTT-S International Microwave Workshop Series on Advanced Material and Processes for RF and THz Applications,* Chengdu, China, 20-22 July, 2016, pp. 1-4.

[139] A. R. Lavado, L. E. Garc´ıa-Mu˜noz, A Generalov, D. Lioubtchenko, K. A. Abdalmalak, S. L. Romano, A Garc´ıa-Lamp´erez, D. S. Vargas, and Antti V. R¨ais¨anen, "Design of a dielectric rod waveguide antenna array for millimeter waves", *Journal of Infrared, Millimeter and Terahertz Waves,* vol. 38, no. 1, pp. 33–46, 15 Sept. 2016.

[140] A. R. Lavado, S. Peu, L. E. Garcia-Muñoz, A. Generalov, J Montero-de-Paz, G. Döhlu, D. Lioubtchenko, M . Méndez-Allen, F. Sedlmein, M. Schneidereit, H.G.L. Schevefel, S. Malzer, D. Segovia-Vargas, and A.V. Räisänen, "Dielectric rod waveguide antenna as THz emitter for photomixing devices", *IEEE Transactions on Antennas and Propagation,* vol. 63, no. 3, pp. 882-890, March 2015.

[141] H. S. Ghadikolaei, C. Fischione, G. Fodor, P. Popovski, M. Zorzi, "Millimeter wave cellular networks: A MAC layer perspective", *IEEE Transactions on Communications*, vol. 63, no. 10, pp. 3437-3458, Oct 2015.

[142] S. Kutty and D Sen, "Beamforming for millimeter wave communications: An inclusive survey", *IEEE Communications Surveys & Tutorials*, vol. 18, no. 2, pp. 949-973, 2016.

[143] J. Mietzner, R. Schober, L. Lampe, W. H. Gerstacker, and P. A. Hoeher, "Multiple antenna techniques for wireless communications—A comprehensive literature survey," *IEEE Commun. Surveys Tuts.*, vol. 11, no. 2, pp. 87–105, Jun. 2009.